MiR-1253 Potentiates Cisplatin Response in Pediatric Group 3 Medulloblastoma by Regulating Ferroptosis

Ranjana K. Kanchan[1], Naveenkumar Perumal[1], Parvez Khan[1], David Doss[1,2], Ramakanth Chirravuri Venkata[1], Ishwor Thapa[3], Raghupathy Vengoji[1], Jyoti B. Kaushal[1], Jawed A. Siddiqui[1], Mohd Wasim Nasser[1], Surinder K. Batra[1], and Sidharth Mahapatra [1,4]

[1] Department of Biochemistry, University of Nebraska Medical Center, Omaha, NE 68198, U.S.A
[2] School of Medicine, Creighton University, Omaha, NE 68178, USA
[3] School of Interdisciplinary Informatics, University of Nebraska at Omaha, Omaha, NE 68182, U.S.A.
[4] Department of Pediatrics, University of Nebraska Medical Center, Omaha, NE 68198, U.S.A.

Corresponding author: Sidharth Mahapatra, MD, PhD, Department of Pediatrics, University of Nebraska Medical Center, 601 South Saddle Creek Road, Omaha, Nebraska, email: sidharth.mahapatra@unmc.edu

Author contributions: RKK and SM conceptualized and designed the study. RKK, JBK and NP performed all experiments. PK developed ABCB7 knockout clone for the study. DD, RCV, and IT provided bioinformatics support for the study. SM coordinated and supervised data analysis. RKK wrote the first draft of the manuscript. NP, PK, DD, RCV, JAS, RV, MWN SKB and SM provided scientific feedback, critical reviews, and helped in revision of the manuscript. All authors have read and approved the final manuscript.

Funding Information: This work was supported by the National Institutes of Health (NICHD K12HD047349); the Edna Ittner Pediatric Research Support Fund; and the Team Jack Brain Tumor Foundation.

Conflicts of Interest: Authors declare that they have no competing interests**.**

Abbreviations: ABC, ATP binding cassette; ANOVA, analysis of variance; BLC-2, B-cell lymphoma 2; BRCA1, breast cancer gene 1;CB, cerebellum; CD276, cluster of differentiation 276 (B7-H3); CDK6, cyclin-dependent kinase 6; c-Myc, c-myelocytomatosis oncogene; DDR, DNA damage repair; DCFDA, 2′,7′-Dichlorofluorescin diacetate; DFO, deferoxamine; FACs, fluorescence-activated cell sorting; FISH, fluorescence *in situ* hybridization; GPX4, glutathione peroxidase 4; GSH, glutathione; GSS, glutathione synthetase; IC_{50}, 50% inhibitory concentration; IHC, immunohistochemistry; i(17q), isochromosome 17q; KEGG, Kyoto encyclopedia of genes and genomes; KO, knock-out; LIP, labile iron pool; LPO, lipid peroxidation; MB, medulloblastoma; MDR, multiple drug resistance; miR, microRNA; miR-1253, microRNA 1253; MnTBAP, Mn(III)tetrakis(4-benzoic acid)porphyrin; mtROS, mitochondrial reactive oxygen species; MTT, 3-(4,5-dimethylthiazol-2-yl)-2,5-diphenyltetrazolium bromide; NC, negative control; NHA, normal human astrocytes; Non-SHH/WNT, non-Sonic Hedgehog/non-Wingless; PARP, poly ADP ribose polymerase; PCR, polymerase chain reaction; Ped, pediatric; PNET, primitive neuro-ectodermal tumor; ROS, reactive oxygen species; RSL3, RAS-selective lethal; SHH, Sonic Hedgehog; WNT, Wingless; XIAP, X-linked inhibitor of apoptosis; XTT, sodium 3′-[1-[(phenylamino)-carbony]-3,4-tetrazolium]-bis(4-methoxy-6-nitro)benzene-sulfonic acid hydrate

Abstract

Medulloblastoma (MB), the most common malignant pediatric brain tumor and a leading cause of childhood mortality, is stratified into four primary subgroups, WNT (wingless), SHH (sonic hedgehog), group 3, and group 4. Patients with group 3 tumors have the poorest prognosis. Loss of 17p13.3, which houses the tumor suppressor gene miR-1253, is a frequent high-risk feature of group 3 tumors.. In this study, we show that miR-1253 levels can disrupt iron homeostasis, induce oxidative stress and lipid peroxidation, triggering an iron-mediated form of cell death called ferroptosis. *In silico* and *in vitro* analyses of group 3 tumors revealed deregulation of ABCB7, a mitochondrial iron transporter and target of miR-1253, and GPX4, a critical regulator of ferroptosis. Restoration of miR-1253 levels in group 3 cell lines resulted in downregulation of ABCB7 and GPX4, consequently increasing cytosolic and mitochondrial labile iron pools, reducing glutathione levels, in turn, resulting in mitochondrial oxidative stress and lipid peroxidation. Together, these events accelerated cancer cell death. Treating miR-1253-expressing cancer cells with cisplatin potentiated cell death by further elevating oxidative stress, depleting glutathione levels, and augmenting lipid peroxidation, with added inhibitory effects on cell viability and colony formation. Treatment with a ferroptosis inhibitor (ferrostatin-1) lead to recovery from the cytotoxic effects of this combination therapy. Together, these findings reveal a novel role for miR-1253 in enhancing ferroptosis to attenuate group 3 tumor cell growth. Our studies provide a proof-of-concept for using miR-based therapeutics to augment current chemotherapeutics in high-risk tumors. Leveraging the tumor-suppressive properties of miRNAs as adjuncts to chemotherapy may provide a promising alternative to current therapeutic strategies.

Key words: ABCB7; ferroptosis; GPX4; medulloblastoma; miR-1253; ROS

Introduction

Of the primitive neuro-ectodermal tumors (PNET) afflicting the posterior fossa, medulloblastoma (MB) is the most common malignant tumor of childhood, accounting for 85% of PNETs and 20% of all posterior fossa tumors.[1-3] Based on high-throughput gene profiling studies, MBs are stratified into four major molecular subgroups: WNT, SHH, group 3 and group 4.[4] Among these, patients with group 3 tumors suffer the worst prognosis (5-year overall survival <50%) due to a highly aggressive phenotype punctuated by c-Myc amplification, haploinsufficiency of chromosome 17p, presence of metastatic lesions at diagnosis, and high rates of recurrence.[4-10] Recurrence can further reduce 5-year overall survival to <10% and is partially fueled by the inability of young patients to tolerate effective chemo- and/or radiation therapy.[4, 11-13] For instance, systemic toxicity is an oft-cited justification for limitations in cisplatin dosing, especially for group 3 disease, leading to <20% of treated patients receiving an effective dose.[14-16] These facts underscore the urgent need to develop new strategies for high risk disease.

Recently, combining microRNAs with chemotherapy has garnered support in enhancing therapeutic efficacy via targeting critical regulators of DNA damage repair (DDR), apoptosis, or cell cycle.[17] In breast cancer, for example, miR-9 and miR-218 improved cisplatin responsiveness by targeting BRCA1 and impeding DNA damage repair.[18, 19] The miR-15 family sensitized cisplatin-resistant cancer cells to apoptosis by targeting the G_2/M cell cycle checkpoint.[20] In gastric and lung cancer cell lines, the miRNA cluster miR-200bc/429 sensitized resistant cell lines to both vincristine and cisplatin by targeting BCL2 and XIAP.[21] In a gemcitabine-resistant pancreatic xenograft model, miR-205 delivered with gemcitabine in conjugated micelles resulted in significant tumor growth inhibition.[22] Most notably, miR-34a

replacement therapy (MRX34) has reached a phase 1 clinical trial (NCT01829971) in patients with primary unresectable or metastatic liver cancer.[23]

Group 3 tumors have amongst the highest frequency of cytogenetic aberrations targeting the short arm of chromosome 17 compared to the other subgroups, with punctuated incidence reported on locus 17p13.3.[24-27] We recently revealed strong tumor suppressive properties for miR-212 and miR-1253 which reside on locus 17p13.3.[27, 28] We showed that miR-1253 directly targets the cell cycle checkpoint protein, CDK6, and CD276 (B7-H3), an immune checkpoint molecule implicated in tumor aggressiveness. [27, 29, 30] Aside from reducing tumor cell viability, migration/invasion, and colony formation, miR-1253 arrested cells at the G_0/G_1 phase, activated apoptotic pathways, and triggered oxidative stress.[27] Numerous studies have recapitulated these strong tumor suppressive properties in various cancers, including non-small cell lung carcinoma[31], osteosarcoma[32], pancreatic cancer[33], male breast cancer[34], and colon cancer[35].

Of interest, the ATP-binding cassette (ABC) family of transporters are known to confer multi-drug resistance to a number of tumor types.[36, 37] These ABC transporters are amongst the novel targets of miR-1253. In metastatic breast cancer, for example, miR-1253 was shown to inhibit the drug efflux pump, ABCB1, thereby potentiating the cytotoxicity of doxorubicin.[38] However, this particular ABC transporter is not amongst the deregulated ABC transporters reported in group 3 MB.[39] Another putative target of miR-1253 is ABCB7, an iron transporter residing on the inner mitochondrial membrane involved in iron homeostasis and Fe-S cluster biogenesis.[40] Deregulation of ABCB7 has been shown to help cancer cells withstand apoptosis and ferroptosis.[41] Ferroptosis is a form of cell death triggered by iron-mediated oxidative stress leading to lethal lipid peroxidation. This process is tightly controlled by glutathione

peroxidase 4 (GPX4), whose primary substrate is the anti-oxidant, glutathione (GSH).[42-44] Recent studies have identified ferroptosis mitigation in tumor progression and drug resistance.[45, 46]

Of the standard chemotherapeutic agents used in the treatment of MB, cisplatin, a platinum-based agent that induces DNA damage, has been shown to trigger cell death via oxidative stress and ferroptosis.[45, 47] Whether deregulation of ABCB7 leads to cisplatin resistance in group 3 tumors or if miR-1253 can sensitize cisplatin response through inhibition of ABCB7 remains unstudied. Thus, we hypothesized that by targeting and inhibiting ABCB7, miR-1253 can induce iron imbalance, oxidative stress, and trigger ferroptosis also potentiating the cytotoxicity of cisplatin in group 3 MB.

Materials and Methods

Patient Samples

Formalin fixed paraffin embedded tissue blocks and frozen tissues of normal cerebellum (pediatric=12, adult=5) and pediatric MB specimens (WNT=1, SHH=9, grp 3=11, grp 4=16, unknown=7) were obtained from the Children's Hospital and Medical Center, Omaha and the University of Nebraska Medical Center after Institutional Review Board approval. Informed consent was not required since the status of the study was exempted. For expression profiles of ABCB7 and GPX4, we cross-analyzed two primary MB datasets (Kanchan *et al.*, GSE148390 and Weishaupt *et al*., GSE124814).[48-50] For Spearman correlation, we used GSE148390. For Kaplan-Meier Survival Analysis, we used the R2 database (Cavalli *et al.*, GSE85217).[9]

Cell Lines and Cell Culture

D283 and D341 were purchased from ATCC (Manassas, Virginia); D425 and D556 were kind gifts from Darell Binger (Duke University Medical Center, Durham, NC); HDMB03 cells were a kind gift from Till Milde (Hopp Children's Tumor Center, Heidelberg, Germany). Cell line genotyping was verified using short tandem repeat (STR) DNA profiling (UNMC). D283, D341, D425 and D556 cell line were maintained in DMEM supplemented with 10%-20% FBS and 100µg/ml penicillin/streptomycin. Normal human astrocytes (NHA) were purchased from Lonza Bioscience (Walkersville, MD) and grown in ABM basal medium supplemented with growth factors (Lonza Biosciences). All cell lines were maintained in 95% humidity, 37°C, 5% CO_2.

Transient Transfections

Cells at a density of 0.5 x 10^6 were seeded in 6-well plates for 24 h and subsequently serum starved for 4 h prior to transfection. Cells were transfected with miR-1253 mimic (miRVanaTM

145 miRNA mimic, ThermoFisher, 100 nM) or scramble negative control (100 nM) with
146 Lipofectamine 2000 (Invitrogen) for 24 h.

147 **CRISPR/Cas9 Knockouts**

148 Lentiviral particles were prepared by transfection of plasmid expressing Cas9 or sgRNA of
149 ABCB7 (Addgene) co-transfected with pCMV-dR8.2 dvpr (Addgene) and pCMV-VSV-g
150 (Addgene) lentiviral packaging plasmids into HEK293T cells using polyethyleneimine (PEI)
151 transfection reagent. Virus-containing supernatant was collected and filtered 48 h after
152 transfection. HDMB03 cells in 6-well plates were infected with Cas9 viral supernatant
153 containing 4 μg/mL polybrene. Following blasticidin selection (10 μg/ml), the expression of
154 Cas9 was confirmed by Western blotting. Stable HDMB03 cells expressing Cas9 expression
155 were infected with the ABCB7 sgRNA viral supernatant containing 4 μg/ml polybrene. After 24
156 h of infection, cells were selected with 0.5 μg/ml puromycin. Single cell clones with Cas9
157 expression and ABCB7 knockout were amplified and used for subsequent experiments.

158 **Cell Viability**

159 After transfection, HDMB03 cells (5 x 10^3 cells/well) were re-seeded into 96-well plates and
160 treated with defined concentrations of cisplatin (1-50 μM) for 24-72 h. Subsequently, MTT (5
161 mg/mL) or XTT (0.3 mg/mL) was added to each well and incubated for 2 or 6 h, respectively, at
162 37 °C. MTT absorbance was measured at 570 nm; XTT absorbance was measured at 440 nm.
163 Data were analyzed using the SOFTMAX PRO software (Molecular Devices Corp., Sunnyvale,
164 CA, USA).

165 **Colony Formation**

166 After transfection, HDMB03 cells (1 x 10^3 cells/well) were re-seeded in 6-well plates. Cells were
167 treated with cisplatin (2 μM) and grown in complete medium for 9 days. Colonies were stained

with 0.25% crystal violet (dissolved in 50% methanol) for 30 min. Crystal violet was dissolved in 10% acetic acid and absorbance read at 590 nm.

Luciferase Assay

Luciferase assay was performed as previously described.[27] Primers ABCB7 Forward: 5'-TAAGCCTGACATAACGAGGA-3'; ABCB7 Reverse: 5'-GCATCTCAGTATTAACTCTAGC -3') were purchased from Eurofins. 3'UTR Wild and 3'UTR-Mutant were incorporated into XbaI restriction site of PGL3-control vector (Promega) expressing firefly luciferase. Dual luciferase assay was done in HDMB03 cells (3 x 10^5cells/well) in 12-well plates. Luciferase activity was the measured using Dual-Luciferase Reporter Assay System (Promega) with a Luminometer (Biotek).

Calcein AM Staining

Calcein-acetoxymethyl ester (Calcein AM) is a membrane permeable, non-fluorescent dye which emits green fluorescence once internalized into the live cells and cleaved by cytoplasmic esterase. Although calcein fluorescence is stable, it can be quenched by divalent metal ions such as iron and cobalt. To estimate cytosolic labile iron pool (LIP), HDMB03 and D425 cells were either transfected with scramble or miR-1253 or had ABCB7 knocked down. Cells were reseeded on to glass coverslips treated with or without the iron chelator deferoxamine (DFO) for 6 h. Cells were washed twice with 0.5 ml of PBS and incubated with 0.05 μM Calcein AM for 15 min at 37 °C. Cells were analyzed under confocal microscope. Ex/Em = 488 nm/525 nm.

Detection of Cytosolic and Mitochondrial Fe^{2+}

Scramble vs. miR-1253-transfected cells or wild-type vs. $ABCB7^{KO}$ cells were seeded onto glass coverslips and were treated with or without DFO (100 μM) for 6 h. For cytosolic LIP, 1 μmol/L FerroOrange (Dojindo, Japan) and 100 nM MitoTraker™ Deep Red FM were added to each

well; for mitochondrial LIP, 1 µM/L Mito-FerroGreen (Dojindo, Japan) and 100 nM MitoTraker Deep Red FM were added to each well. Cells were incubated in a 37^{o} C incubator equilibrated with 95% air and 5% CO_2 for 30 min. After incubation cells were washed and counter-stained with 4′,6-diamidino-2-phenylindole (DAPI). Cells were observed under a confocal fluorescence microscope, $Ex/Em_{cytosolicLIP}$ = 561 nm/570-620 nm, $Ex/Em_{mitochondrialLIP}$ = 488 nm/500-550 nm.

Measurement of Intracellular Oxidative Stress

Intracellular ROS (H_2O_2) was measured using oxidation-sensitive fluorescent probe 2′,7′-Dichlorofluorescin diacetate (DCFDA) (Sigma Aldrich, USA); mitochondrial $O_2^{\bullet -}$ was measured using MitoSOX™ Red (Thermofisher, USA). Scramble vs. miR-1253-transfected cells or wild-type vs. $ABCB7^{KO}$ cells were treated with cisplatin or cisplatin and Ferrostatin-1 (Apexbio, USA) for 24 h. Cells were incubated with 10 µM DCFDA or 5 µM MitoSOX™ Red for 30 min. Oxidized DCFDA and MitoSOX™ Red were measured using at Ex/Em ~485/528 nm and Ex/Em ~510/580, respectively.[51] Images were captured using EVOS FL Auto Imaging System (EVOS FL Auto, Life Technologies). Oxidized DCFDA and MitoSOXRed were measured using multimode plate reader at Ex/Em ~485/528 nm and Ex/Em ~510/580, respectively

Measurement of Lipid Peroxidation

The Image-iT® LPO kit was used to measure lipid ROS through oxidation of the C-11-BODIPY® 581/591 sensor according to the manufacturer's instructions. Briefly, scramble vs. miR-1253-transfected cells or wild-type vs. $ABCB7^{KO}$ cells were treated with or without cisplatin or a combination of cisplatin and Ferrostatin-1 for 24 h. Cells were then stained with Image-iT® Lipid Peroxidation Sensor (10 µM) for 30 min and counter-stained with DAPI. Images were captured by confocal microscopy.

Ferroptosis Assessment by Flow Cytometry

Scramble and miR-1253-transfected cells were treated with or without cisplatin or a combination of cisplatin and Ferrostatin-1 for 24 h. After completion of treatment, cells were incubated with 5 µM of MitoSOX™ Red for 30 min. Cells were washed and stained with Annexin-V/Cy™5(BD Biosciences). Cell populations were sorted and measured by flow cytometry.

Glutathione Estimation

Glutathione estimation was performed according to the manufacturer's instructions using GSH-Glo™ Glutathione Assay kit (Promega, USA). Briefly, scramble vs. miR-1253-transfected cells or wild-type vs. $ABCB7^{KO}$ cells were seeded (5×10^3 cells/well) in the 96-well plates. Cells were treated with or without cisplatin or in combination with cisplatin and Ferrostatin-1 for 24 h. Plates were incubated in the dark for 30 min on a plate shaker with 100 µl of prepared 1x GSH-Glo™ Reagent. Then, 100 µl of reconstituted Luciferin Detection Reagent was added to each well and incubated in the dark for another 15 min. A standard curve was prepared using GSH standard solution to facilitate the conversion of luminescence to GSH concentration.

Immunofluorescence Imaging

In cultured cells: scramble vs. miR-1253-transfected cells or wild-type vs. $ABCB7^{KO}$ cells were seeded onto coverslips, rinsed, and fixed using 4% paraformaldehyde (PFA) in PBS for 10 min at room temperature. Cells were washed, incubated with 0.25% Triton X-100, and blocked with 3% BSA at room temperature. Cells were then incubated with primary antibody ABCB7 or COXIV overnight. Following day, cells were incubated with Alexafluor 488 and Alexaflour 547 conjugated antibodies for 1 h. Cells were washed and counter stained with DAPI. Images were captured at 63X using Carl Zeiss microscope (LSM 800 META).

In tissue: immunofluorescence was performed on surgically-resected, formalin-fixed, paraffin-embedded sections of group 3 medulloblastomas. Deparaffinized tissue sections were blocked

with 5% BSA after heat induced epitope retrieval with citrate buffer (pH 6.0) and then incubated with primary antibodies, ABCB7 rabbit monoclonal antibody (1:200), GPX4 rabbit monoclonal antibody, or COXIV mouse monoclonal antibody (1:200). Following overnight incubation with primary antibody, sections were incubated for 1 h with Alexa-488 or Alexa-547-conjugated, mouse and rabbit secondary antibodies (1:200). Sections were counter-stained with DAPI. Micrographs were captured at 20X using Carl Zeiss microscope (LSM 800 META).

PCR Primers

Total RNA extraction and quantitative PCR (qPCR) were performed according to manufacturer protocol. The forward (F) and reverse (R) primer sequences were as follows: ABCB7 (F): 5'-AAGATGTGAGCCTGGAAAGC-3' (R): 5'- AGAGGACAGCATCCTGAGGT-3'; GPx4 (F): 5'-ACAAGAACGGCTGCGTGGTGAA-3' (R): 5'-GCCACACACTTGTGGAGCTAGA-3'; β-Actin (F): 5'-CACCATTGGCAATGAGCGGTTC-3'(R): 5'-AGGTCTTTGCGGATGTCCACGT-3'.

Statistical Analysis

Data are presented as mean ± SD. All experiments were conducted at least in duplicates with 3-6 replicates per experiment. Statistical analyses were performed using Prism 9.2 (GraphPad Software). Differences between groups were compared using Student's t-test or one-way analysis of variance (ANOVA). Statistical significance was established at $*p < 0.05$; $**p < 0.01$; $***p < 0.001$; $****p < 0.0001$. Statistical analyses of high-throughput sequencing data were performed using R Statistical Software v4.1.1 (R Core Team), expression values were compared using a Mann-Whitney *U* test.

Results

ABCB7, a novel target of miR-1253, is deregulated in group 3 medulloblastomas.

In our previous study, we identified miR-1253 as a novel tumor suppressor gene in MB and its multiple oncogenic targets.[27] Here, we sought to determine other targets of miR-1253, especially those that may regulate drug sensitivity in MB. Upon restoration of miR-1253, using transient overexpression in HDMB03 cells, we observed potent negative regulation of the ABC transporter superfamily by KEGG pathways and RNA Sequencing analyses (**Supplementary Figures 1A** and **1B**). We wanted to then isolate specific targets of miR-1253 relevant to group 3 MB pathophysiology and/or aggressiveness. We began by identifying ABC transporters deregulated in group 3 MB (**Supplementary Figure 1C**, column 1). From this list, we isolated transporters whose deregulated expression in group 3 MB conferred poor prognosis (**Supplementary Figure 1C**, column 2, **red**). Within this cohort, we examined transporters whose expression was negatively impacted by stable miR-1253 overexpression in HDMB03 cells (**Supplementary Figure 1C**, column 3). This comparative analysis revealed ABCB7 as the best putative miR-1253 target for further study.

We first learned that ABCB7 was in fact deregulated in multiple MB cohorts with high expression conferring a poor prognosis (**Supplementary Figures 1D** and **1E**). By comparing subgroup-specific ABCB7 expression in 3 recent MB cohorts, we identified consistent deregulation of ABCB7 in group 3 tumors (**Figure 1A** and **Supplementary Figure 1F** and **1G**). We further observed a strong association of ABCB7 deregulation with tumor aggressiveness, impacting overall survival of group 3 MB patients (**Figure 1B**). Next, we confirmed high expression of ABCB7 in our local cohort of group 3 tumors and its co-localization within the inner mitochondrial membrane as evidenced by COXIV staining by confocal microscopy

(**Figure 1C**). Additionally, we confirmed relatively high expression of ABCB7 in a panel of aggressive group 3 MB cell lines when compared to normal human astrocytes (**Figure 1D**).

To demonstrate ABCB7 targeting by miR-1253, we first showed translational repression via Western blotting in 2 group 3 MB cell lines, D425 (**Figure 1E**) and HDMB03 (**Figure 1F**). In the same cell lines, confocal imaging showed both localization of ABCB7 to the inner mitochondrial membrane and visualized the effects of miR-1253 expression on ABCB7 expression inhibition, as evidenced by a dramatically reduced green fluorescence (**Figure 1G**). Finally, we showed direct binding of miR-1253 to ABCB7 via a dual-luciferase reporter assay (**Figures 1H**). Taken together, these data confirmed ABCB7 as a direct target of miR-1253 and strongly implicated its deregulation as a poor prognostic marker specific to group 3 MB.

MiR-1253 triggers iron imbalance and oxidative stress leading to cell death in group 3 MB cell lines.

ABCB7 plays a critical role in maintaining intracellular iron stores.[52] Residing on the inner mitochondrial membrane, it homodimerizes to deliver Fe-S clusters synthesized within the mitochondria to the cytoplasm.[52-54] To determine the effect of ABCB7 inhibition via miR-1253 on iron homeostasis, we studied accumulation of free ferrous iron (Fe^{2+}) within the mitochondria and the cytosol in miR-1253-transfected cells. Calcein AM is a membrane permeable dye which produces green fluorescence when internalized and can be rapidly quenched by divalent metals (iron, cobalt, cadmium). MiR-1253 expression in D425 and HDMB03 cells led to quenching of Calcein AM dye when compared with untransfected cancer cells (**Figure 2A** and **2B**).

We further compared the fluorescence of FerroOrange (specific for cytosolic Fe^{2+})[55] and Mito-FerroGreen (specific for mitochondrial Fe^{2+})[56] in these systems and observed an increase

in fluorescence intensity for both in miR-1253-transfected HDMB03 cells as compared to untransfected control cells (**Figure 2C**). Treatment with an iron chelator, deferoxamine (DFO), reduced fluorescence to normal levels in these cells, substantiating the generation of a labile iron pool in both the mitochondria and cytoplasm with miR-1253 expression.

Disrupting iron homeostasis can lead to excessive reactive oxygen species (ROS) generation by the Fenton reaction, targeting cellular lipids, proteins, and nucleic acids, eventuating in cellular damage and death.[57, 58] Superoxide ($O_2^{\bullet -}$) and hydrogen peroxide (H_2O_2) are the major species generated by the mitochondria during oxidative phosphorylation.[59] To investigate the consequence of triggering free ferrous iron accumulation, we measured mitochondrial and cytosolic ROS (MitoSOX^{TM} RED and DCFDA, respectively) and subsequent lipid peroxidation in miR-1253-transfected cells. Both mitochondrial $O_2^{\bullet -}$ and cytosolic H_2O_2 levels increased significantly in miR-1253-transfected D425 (**Figure 3A**) and HDMB03 (**Figure 3B**) cells. This was concurrent with an increase in lipid peroxidation in miR-1253-transfected cell lines (**Figures 3C** and **3D**).

Ferroptosis is defined as an iron-dependent form of regulated cell death resulting from lipid peroxidation.[42] Given our observations with iron accumulation, ROS generation, and lipid peroxidation, we wanted to assess whether miR-1253 can, in fact, trigger ferroptosis. D425 and HDMB03 cells transfected with miR-1253 were stained with MitoSOX™ Red (for $O_2^{\bullet -}$) and Annexin-V/Cy™5 (marker of apoptotic cell death). Flow cytometry analysis revealed a significant (~3-fold) rise in dual-stained cells (Q2) indicating oxidative stress-mediated cell death (**Figure 3E** and **3F**). Collectively, our findings revealed that miR-1253 can trigger iron accumulation within the mitochondria and cytosol, resulting in oxidative stress and lipid peroxidation, eventually leading to cell death by ferroptosis.

Knocking out ABCB7 can also trigger iron imbalance and oxidative stress in group 3 MB cell lines.

Given the central role ABCB7 plays in iron homeostasis, we conducted similar studies in ABCB7^{KO} HDMB03 cells. First, we generated the knockout (KO) cell line using CRISPR/Cas9 technology (**Figure 4A** and **4B**). As prior, we studied iron imbalance via Calcein AM dye quenching and FerroOrange and Mito-FerroGreen fluorescence via confocal microscopy. As expected, we recapitulated findings from miR-1253-transfected cancer cells in ABCB7^{KO} cells (**Figures 4C-F**). Together, these studies confirmed that the miR-1253-mediated induction of ferroptosis was strongly contributed by ABCB7 targeting.

MiR-1253 and ABCB7 influence GPX4 expression, a key regulator of ferroptosis.

Glutathione (GSH) serves as a cell's primary antioxidant, capable of binding to Fe^{2+} to prevent iron-mediated oxidative stress.[42, 60] It also serves as the main substrate for glutathione peroxidase 4 (GPX4), a critical player in the elimination of toxic lipid peroxides engendered from oxidative stress that can trigger ferroptosis (**Figure 5A**). In patients with cancer, GPX4 is often deregulated, purportedly by epigenetic mechanisms, and has been shown to correlate not only with poor prognosis but also increased drug resistance. Consequently, inhibition of GPX4 by RAS-selective lethal 3 (RSL3) was noted to sensitize lung cancer cells to cisplatin.[47] Similarly, in neuroblastoma, withaferin A induced ferroptosis and tumor growth suppression by inhibiting GPX4.[61]

In MB, we noted a significant deregulation of GPX4 in all tumor subtypes, with the highest expression noted in group 3 MB (**Figure 5B** and **Supplementary Figure 2**); prognosis in high-expressing patients was poor (**Figure 5C**). Immunofluorescence studies revealed high expression of GPX4 in group 3 MB and co-localization of GPX4 to the mitochondria (**Figure 5D**). In

classic group 3 MB cell lines, GPX4 expression was significantly elevated compared to normal human astrocytes (**Figure 5E**).

We then studied the influence of miR-1253 and ABCB7^{KO} on GPX4 levels. As demonstrated, GPX4 levels were reduced in miR-1253-expressing D425 and HDMB03 cells (**Figure 5F**). Notably, with ABCB7^{KO}, GPX4 expression was almost completely abrogated. Similarly, we noted a positive Pearson correlation (R=0.43, p =0.023) between GPX4 and ABCB7 (**Figure 5G**). GSH, a main substrate of GPX4, was concurrently reduced in miR-1253-overexpressing D425 and HDMB03 cells (**Figure 5H**). Together, these findings revealed the effects of miR-1253 on GPX4 regulation and GSH levels in its contribution to ferroptosis.

Restoration of miR-1253 potentiates cisplatin cytotoxicity in group 3 MB cell lines.

Cisplatin, a platinum-containing chemotherapeutic agent, induces DNA damage via various mechanisms, including (i) crosslinking DNA purine bases, (ii) inducing oxidative stress, and (iii) interfering with DNA repair machinery, that can eventually lead to cancer cell death.[62] It is also the only agent used in group 3 MB that possesses ferroptotic potential.[45, 63] Given the induction of apoptotic and ferroptotic cell death by miR-1253, we next investigated if miR-1253 can potentiate cisplatin response in group 3 MB. We first determined the IC_{50} of cisplatin in scramble vs. miR-1253-transfected D425 (**Figure 6A**) and HDMB03 (**Figure 6B**) cells. In both cell lines, miR-1253 restoration lowered the IC_{50} by ~2-fold (**Figure 6C**). We then performed colony formation assays with the IC_{25} of cisplatin in HDMB03 cells (24 h: 2 μM) and noted a complete abrogation of colonies in miR-1253-expressing cells (**Figure 6D**).

Eliciting high levels of cellular superoxide is one of the mechanisms by which cisplatin can induce tumor cell death.[64] So, we next investigated whether cisplatin treatment enhances mitochondrial (mtROS) and cytosolic ROS in group 3 MB cells. Using prior fluorescent probes

for mtROS (MitoSOX™ Red) and cytosolic ROS (DCFDA), we studied miR-1253 transfected cells subjected to 10 µM cisplatin in D425 and 2 µM cisplatin in HDMB03 cells at 24 h; we concurrently examined cisplatin treatment (2 µM) of ABCB7^{KO} HDMB03 cells. As prior, miR-1253 expression or ABCB7^{KO} induced significantly higher levels of mtROS and cytosolic ROS compared to control. Moreover, in all cases, miR-1253 potentiated cisplatin-mediated ROS (**Figures 6E-G**). Taken together, these findings not only highlighted the strong ability of miR-1253 to elicit ROS, but also revealed the cisplatin-potentiating action of miR-1253.

Inhibiting ferroptosis rescues cisplatin potentiation by miR-1253 in group 3 MB cells.

We next wanted to confirm that ferroptosis was elicited by miR-1253 alone and potentiated by combination with cisplatin. We systematically looked at mtROS and cytosolic ROS, lipid peroxidation, GSH levels, and levels of apoptotic and ferroptotic cell death in miR-1253-transfected or ABCB7^{KO} cancer cells treated with 1) cisplatin and 2) in combination with ferrostatin-1 (a potent inhibitor of ferroptosis).

First, cisplatin alone induced oxidative stress; addition of ferrostatin-1 to cisplatin treatment led to a dramatic reduction in H_2O_2 but not $O_2^{\bullet -}$. Second, miR-1253 expression or ABCB7^{KO} led to a significant rise in oxidative stress, which was potentiated by the addition of cisplatin; treatment with ferrostatin-1 substantially reduced the generation of both H_2O_2 and $O_2^{\bullet -}$ (**Figures 7A** and **7B**; **Supplementary Figure 3A** and **3B**). Similarly, while cisplatin alone had modest effects on lipid peroxidation, combining it with miR-1253 expression or ABCB7 knockdown resulted in the highest levels of lipid peroxidation; in turn, ferrostatin-1 significantly reduced lipid peroxidation in miR-1253 transfected and ABCB7^{KO} HDMB03 cells (**Figure 7C** and **Supplementary Figure 3C**). Given the central importance of glutathione as an antioxidant, we observed that cisplatin depleted GSH in miR-1253 transfected and ABCB7^{KO} HDMB03 cells

with the addition of ferrostatin having some recovery effects. As prior, cisplatin added to cells with ABCB7 inhibition had the strongest effect in depleting GSH; ferrotstatin-1 catalyzed the recovery of reduced glutathione levels in these cells **(Figure 7D** and **Supplementary Figure 3D**).

Finally, examining O_2-mediated cell death (as a proxy for ferroptosis) at 24 h, cisplatin showed a small rise in ROS-mediated cell death and apoptosis, while miR-1253 led to a larger rise in both. Treating miR-1253-transfected HDMB03 cells with cisplatin accomplished a dramatic increase in both ROS-mediated and apoptotic cell death; ferrostatin-1 treatment rescued the former, strongly implicating the important contribution of ferroptosis to the mechanism of miR-1253-induced cell death . **(Figure 7E)**. Together these data substantiate the cardinal role of miR-1253 in inducing ferroptosis and its potentiating effects on cisplatin cytotoxicity.

Discussion

Amongst the most devastating diagnoses in a pediatric patient is a tumor of the central nervous system, with medulloblastoma being the most common malignant tumor.[3, 4, 65, 66] Punctuated for group 3 MB, poor survival (5-year OS <50%) in these patients is attributable to a combination of young age at diagnosis (peak age 3-5), metastases at diagnosis (up to 50%), and c-Myc amplification.[9, 28, 67-70] Current treatment regimens have yet to impact the dismal prognosis with stagnant survival rates seen over the last decade.[71] An inability to tolerate mainstay of therapy especially for young patients fuels high relapse rates (~30%) which are universally fatal. For example, in children under the age of 4 years relapse was noted in ~60% of patients who did not receive upfront craniospinal irradiation. Moreover, relapse rates were highest in group 3 MB tumors and those with i17q and c-Myc amplification.[72] In those that do manage to survive, irreversible damage to the hypothalamic-pituitary axis is sustained from cytotoxic treatment regimens resulting in short stature, cognitive impairments, and emotional lability.[73, 74] Thus, the need for novel therapeutic strategies that mitigate drug-related cytotoxicity yet accomplish widespread tumor abstraction for this subgroup is dire.

Elevated recurrence rates have often been conjectured to be linked to mechanisms for drug resistance in group 3 MB, which may include high expression of multi-drug resistance (MDR) genes belonging to the ABC transporter family.[36, 37, 39, 75, 76] Cytotoxic drugs, in combination with tumor suppressive miRNAs, have the potential for a more complex and profound effect on tumorigenesis and may possess the ability to address drug resistance patterns, especially if they can target MDR genes.[77] Here, we demonstrated a strong negative enrichment of the ABC transporter family with miR-1253 expression restoration in group 3 MB cells. Of the multiple transporters identified via our bioinformatics approach, we isolated

ABCB7, whose deregulated expression profile in group 3 tumors was strongly associated with poor prognosis, as a target of miR-1253.

ABCB7 is an iron transporter residing on the inner mitochondrial membrane and involved in Fe-S cluster biogenesis.[53, 78] ABCB7 deficiency can lead to decreased expression of electron transport chain (ETC) complex proteins I, II, IV and V, which can trigger impaired oxidative phosphorylation and mitochondrial membrane integrity resulting in oxidative stress.[40, 79-81] In glioma cells, inhibition of ABCB7 resulted in disruption of iron transport and ROS generation triggering apoptotic and non-apoptotic cell death.[41] Iron accumulation can trigger oxidative stress and vice versa[82, 83], resulting in lethal lipid peroxidation activating ferroptosis, which is distinct from apoptosis, necrosis, autophagy, and pyroptosis.[84]

With a strong premise for exploring iron imbalance through miR-1253, our subsequent results substantiated a ferroptotic role for miR-1253 in MB. First, miR-1253 induced intracellular iron accumulation in D425 and HDMB03 cells, effectively abrogated by pre-treatment with an iron chelator, DFO. $ABCB7^{KO}$ resulted in a similar phenotype. This resulted in elevated mitochondrial ROS ($O_2^{\bullet -}$) and cytosolic ROS (H_2O_2). We also recorded a high lipid oxidation profile in these cell lines concurrent with miR-1253 expression. Finally, using AnnexinV and MitoSOX™ Red staining, we revealed a significantly elevated dual staining population of cells in miR-1253-expressing cells. Taken together, these results are highly indictive of ferroptosis induction by miR-1253 in group 3 MB cells.

Ferroptosis can also be induced by disruption of glutathione synthesis or inhibition of glutathione peroxidase 4.[85] Cancer cells have the capacity to activate redox buffering systems to survive in a highly oxidative environment resulting from deregulated cellular functions.[86] Glutathione is a key player in this response and a critical cofactor for glutathione peroxidase 4

(GPX4). GPX4, a central regulator of ferroptosis upregulated in various cancers, uses glutathione to reduce ROS and lipid hydroperoxide levels thus facilitating tumor cell survival in an environment with high oxidative stress.[87] Additionally, GSH binds Fe^{2+} to prevent iron oxidation and is thus a critical component controlling the labile iron pool.[60] Of note, ABCB7 harbors a GSH binding pocket, and GSH is a required substrate for cytosolic and nuclear Fe-S protein biogenesis and iron homeostasis.[52, 88] In group 3 tumors, we not only showed deregulated GPX4 expression but also a strong positive correlation with ABCB7. Resultantly, miR-1253 expression or $ABCB7^{KO}$ strongly inhibited GPX4 expression and reduced glutathione levels. These data demonstrate the contribution of disrupting GPX4 and glutathione metabolism in miR-1253-mediated oxidative stress mechanisms resulting in ferroptosis.

MiRNA mimics have been shown to possess the capability of restoring the sensitivity of cancer cells for chemotherapeutic agents and to thus subsequently enhance their effectiveness. For example, miR-429, miR-383, miR-101-3p, miR-195, miR-634, and miR-1294 elicited a 2-5 fold reduction in the EC_{50} and IC_{50} values in combination with gemcitabine, temozolomide, and paclitaxel.[77, 89-94] Of the standard chemotherapies for medulloblastoma tumors, only cisplatin has been shown to trigger both apoptosis and ferroptosis, via oxidative stress, GSH depletion, and GPX4 inactivation.[45, 47, 63, 64] Moreover, a microarray-based study of the IC_{50} of cisplatin in 60 NCI cell lines identified multiple ABC transporters, including 3 iron transporters, i.e. ABCB6, ABCB7 and ABCB10, in conferring cisplatin drug resistance.[95]

Given the ferroptotic mechanism we elucidated for miR-1253, we studied whether miR-1253 expression can potentiate cisplatin cytotoxicity in group 3 MB cells. We report a 2-fold reduction in the IC_{50} value of cisplatin with miR-1253 induction in D425 and HDMB03 cells. Combination treatment had dramatic effects on the clonal potential of HDMB03 cells. We then demonstrated

the highest induction of mitochondrial and cytosolic ROS, lipid peroxidation, and GSH depletion in miR-1253-expressing HDMB03 and ABCB7^{KO} HDMB03 cells treated with cisplatin. Consequently, combination therapy resulted in the highest degree of ferroptosis in these cell lines. These effects were reversed by ferrostatin-1, a potent inhibitor of ferroptosis, lending further validity to the central role of ferroptosis in the mechanism of miR-1253-mediated effects and cisplatin potentiation.

Overall, our study has identified novel tumor suppressive properties for miR-1253. First, miR-1253 directly inhibits ABCB7 expression, thus inducing labile iron pool within MB cancer cells and stimulating ROS production. MiR-1253 can concurrently downregulate the expression of GPX4 and deplete GSH, further exacerbating ROS. Together, the generation of lipid hyperoxides progresses unabated, leading to cancer cell death via ferroptosis. We also leveraged these properties by showing potentiation of cisplatin cytotoxicity and thus enhanced therapeutic efficacy in group 3 MB cells. Together, our findings provide proof-of-concept for further exploration of tumor suppressive microRNAs as therapeutic adjuncts to standard chemotherapy. Such a strategy may mitigate the current limitations to treatment regimens in our youngest high risk patients.

References

[1] R.E. Taylor, P.H. Donachie, C.L. Weston, K.J. Robinson, H. Lucraft, F. Saran, D.W. Ellison, J. Ironside, D.A. Walker, B.L. Pizer, C. Children's, C.N.S.T.D. Leukaemia Group, Impact of radiotherapy parameters on outcome for patients with supratentorial primitive neuro-ectodermal tumours entered into the SIOP/UKCCSG PNET 3 study, Radiother Oncol 92(1) (2009) 83-8.

[2] Y.T. Udaka, R.J. Packer, Pediatric Brain Tumors, Neurol Clin 36(3) (2018) 533-556.

[3] Q.T. Ostrom, N. Patil, G. Cioffi, K. Waite, C. Kruchko, J.S. Barnholtz-Sloan, CBTRUS Statistical Report: Primary Brain and Other Central Nervous System Tumors Diagnosed in the United States in 2013-2017, Neuro Oncol 22(12 Suppl 2) (2020) iv1-iv96.

[4] M.D. Taylor, P.A. Northcott, A. Korshunov, M. Remke, Y.J. Cho, S.C. Clifford, C.G. Eberhart, D.W. Parsons, S. Rutkowski, A. Gajjar, D.W. Ellison, P. Lichter, R.J. Gilbertson, S.L. Pomeroy, M. Kool, S.M. Pfister, Molecular subgroups of medulloblastoma: the current consensus, Acta neuropathologica 123(4) (2012) 465-72.

[5] M. Zapotocky, D. Mata-Mbemba, D. Sumerauer, P. Liby, A. Lassaletta, J. Zamecnik, L. Krskova, M. Kyncl, J. Stary, S. Laughlin, A. Arnoldo, C. Hawkins, U. Tabori, M.D. Taylor, E. Bouffet, C. Raybaud, V. Ramaswamy, Differential patterns of metastatic dissemination across medulloblastoma subgroups, J Neurosurg Pediatr 21(2) (2018) 145-152.

[6] P.A. Northcott, A. Korshunov, H. Witt, T. Hielscher, C.G. Eberhart, S. Mack, E. Bouffet, S.C. Clifford, C.E. Hawkins, P. French, J.T. Rutka, S. Pfister, M.D. Taylor, Medulloblastoma comprises four distinct molecular variants, Journal of clinical oncology : official journal of the American Society of Clinical Oncology 29(11) (2011) 1408-14.

[7] D.W. Ellison, M. Kocak, J. Dalton, H. Megahed, M.E. Lusher, S.L. Ryan, W. Zhao, S.L. Nicholson, R.E. Taylor, S. Bailey, S.C. Clifford, Definition of disease-risk stratification groups in childhood medulloblastoma using combined clinical, pathologic, and molecular variables, Journal of clinical oncology : official journal of the American Society of Clinical Oncology 29(11) (2011) 1400-7.

[8] M. Kool, J. Koster, J. Bunt, N.E. Hasselt, A. Lakeman, P. van Sluis, D. Troost, N.S. Meeteren, H.N. Caron, J. Cloos, A. Mrsic, B. Ylstra, W. Grajkowska, W. Hartmann, T. Pietsch, D. Ellison, S.C. Clifford, R. Versteeg, Integrated genomics identifies five medulloblastoma subtypes with distinct genetic profiles, pathway signatures and clinicopathological features, PLoS One 3(8) (2008) e3088.

[9] F.M.G. Cavalli, M. Remke, L. Rampasek, J. Peacock, D.J.H. Shih, B. Luu, L. Garzia, J. Torchia, C. Nor, A.S. Morrissy, S. Agnihotri, Y.Y. Thompson, C.M. Kuzan-Fischer, H. Farooq, K. Isaev, C. Daniels, B.K. Cho, S.K. Kim, K.C. Wang, J.Y. Lee, W.A. Grajkowska, M. Perek-Polnik, A. Vasiljevic, C. Faure-Conter, A. Jouvet, C. Giannini, A.A. Nageswara Rao, K.K.W. Li, H.K. Ng, C.G. Eberhart, I.F. Pollack, R.L. Hamilton, G.Y. Gillespie, J.M. Olson, S. Leary, W.A. Weiss, B. Lach, L.B. Chambless, R.C. Thompson, M.K. Cooper, R. Vibhakar, P. Hauser, M.C. van Veelen, J.M. Kros, P.J. French, Y.S. Ra, T. Kumabe, E. Lopez-Aguilar, K. Zitterbart, J. Sterba, G. Finocchiaro, M. Massimino, E.G. Van Meir, S. Osuka, T. Shofuda, A. Klekner, M. Zollo, J.R. Leonard, J.B. Rubin, N. Jabado, S. Albrecht, J. Mora, T.E. Van Meter, S. Jung, A.S. Moore, A.R. Hallahan, J.A. Chan, D.P.C. Tirapelli, C.G. Carlotti, M. Fouladi, J. Pimentel, C.C. Faria, A.G. Saad, L. Massimi, L.M. Liau, H. Wheeler, H. Nakamura, S.K. Elbabaa, M. Perezpena-Diazconti, F. Chico Ponce de Leon, S. Robinson, M. Zapotocky, A. Lassaletta, A. Huang, C.E. Hawkins, U. Tabori, E. Bouffet, U. Bartels, P.B. Dirks, J.T. Rutka, G.D. Bader, J. Reimand, A. Goldenberg, V. Ramaswamy, M.D. Taylor, Intertumoral Heterogeneity within Medulloblastoma Subgroups, Cancer Cell 31(6) (2017) 737-754 e6.

[10] V. Ramaswamy, M. Remke, E. Bouffet, C.C. Faria, S. Perreault, Y.J. Cho, D.J. Shih, B. Luu, A.M. Dubuc, P.A. Northcott, U. Schuller, S. Gururangan, R. McLendon, D. Bigner, M. Fouladi, K.L. Ligon, S.L. Pomeroy, S. Dunn, J. Triscott, N. Jabado, A. Fontebasso, D.T. Jones, M. Kool, M.A. Karajannis, S.L. Gardner, D. Zagzag, S. Nunes, J. Pimentel, J. Mora, E. Lipp, A.W. Walter, M. Ryzhova, O. Zheludkova, E. Kumirova, J. Alshami, S.E. Croul, J.T. Rutka, C. Hawkins, U. Tabori, K.E. Codispoti, R.J. Packer, S.M. Pfister, A. Korshunov, M.D. Taylor, Recurrence patterns across medulloblastoma subgroups: an integrated clinical and molecular analysis, Lancet Oncol 14(12) (2013) 1200-7.

[11] S. Rieken, A. Mohr, D. Habermehl, T. Welzel, K. Lindel, O. Witt, A.E. Kulozik, W. Wick, J. Debus, S.E. Combs, Outcome and prognostic factors of radiation therapy for medulloblastoma, Int J Radiat Oncol Biol Phys 81(3) (2011) e7-e13.

[12] R.J. Packer, J. Goldwein, H.S. Nicholson, L.G. Vezina, J.C. Allen, M.D. Ris, K. Muraszko, L.B. Rorke, W.M. Wara, B.H. Cohen, J.M. Boyett, Treatment of children with medulloblastomas with reduced-dose craniospinal radiation therapy and adjuvant chemotherapy: A Children's Cancer Group Study, Journal of clinical oncology : official journal of the American Society of Clinical Oncology 17(7) (1999) 2127-36.

[13] A. Gajjar, M. Chintagumpala, D. Ashley, S. Kellie, L.E. Kun, T.E. Merchant, S. Woo, G. Wheeler, V. Ahern, M.J. Krasin, M. Fouladi, A. Broniscer, R. Krance, G.A. Hale, C.F. Stewart, R. Dauser, R.A. Sanford, C. Fuller, C. Lau, J.M. Boyett, D. Wallace, R.J. Gilbertson, Risk-adapted craniospinal radiotherapy followed by high-dose chemotherapy and stem-cell rescue in children with newly diagnosed medulloblastoma (St Jude Medulloblastoma-96): long-term results from a prospective, multicentre trial, The Lancet. Oncology 7(10) (2006) 813-20.

[14] A.M. Martin, E. Raabe, C. Eberhart, K.J. Cohen, Management of pediatric and adult patients with medulloblastoma, Curr Treat Options Oncol 15(4) (2014) 581-94.

[15] J. Enriquez Perez, S. Fritzell, J. Kopecky, E. Visse, A. Darabi, P. Siesjo, The effect of locally delivered cisplatin is dependent on an intact immune function in an experimental glioma model, Sci Rep 9(1) (2019) 5632.

[16] A.A. Nageswara Rao, D.J. Wallace, C. Billups, J.M. Boyett, A. Gajjar, R.J. Packer, Cumulative cisplatin dose is not associated with event-free or overall survival in children with newly diagnosed average-risk medulloblastoma treated with cisplatin based adjuvant chemotherapy: report from the Children's Oncology Group, Pediatr Blood Cancer 61(1) (2014) 102-6.

[17] M. Mognato, L. Celotti, MicroRNAs Used in Combination with Anti-Cancer Treatments Can Enhance Therapy Efficacy, Mini Rev Med Chem 15(13) (2015) 1052-62.

570 [18] X. He, X. Xiao, L. Dong, N. Wan, Z. Zhou, H. Deng, X. Zhang, MiR-218 regulates cisplatin
571 chemosensitivity in breast cancer by targeting BRCA1, Tumour Biol 36(3) (2015) 2065-75.
572 [19] C. Sun, N. Li, Z. Yang, B. Zhou, Y. He, D. Weng, Y. Fang, P. Wu, P. Chen, X. Yang, D. Ma, J.
573 Zhou, G. Chen, miR-9 regulation of BRCA1 and ovarian cancer sensitivity to cisplatin and PARP
574 inhibition, J Natl Cancer Inst 105(22) (2013) 1750-8.
575 [20] L.M. Pouliot, Y.C. Chen, J. Bai, R. Guha, S.E. Martin, M.M. Gottesman, M.D. Hall, Cisplatin
576 sensitivity mediated by WEE1 and CHK1 is mediated by miR-155 and the miR-15 family, Cancer Res
577 72(22) (2012) 5945-55.
578 [21] W. Zhu, H. Xu, D. Zhu, H. Zhi, T. Wang, J. Wang, B. Jiang, Y. Shu, P. Liu, miR-200bc/429 cluster
579 modulates multidrug resistance of human cancer cell lines by targeting BCL2 and XIAP, Cancer
580 Chemother Pharmacol 69(3) (2012) 723-31.
581 [22] A. Mittal, D. Chitkara, S.W. Behrman, R.I. Mahato, Efficacy of gemcitabine conjugated and
582 miRNA-205 complexed micelles for treatment of advanced pancreatic cancer, Biomaterials 35(25) (2014)
583 7077-87.
584 [23] D.S. Hong, Y.K. Kang, M. Borad, J. Sachdev, S. Ejadi, H.Y. Lim, A.J. Brenner, K. Park, J.L. Lee,
585 T.Y. Kim, S. Shin, C.R. Becerra, G. Falchook, J. Stoudemire, D. Martin, K. Kelnar, H. Peltier, V. Bonato,
586 A.G. Bader, S. Smith, S. Kim, V. O'Neill, M.S. Beg, Phase 1 study of MRX34, a liposomal miR-34a
587 mimic, in patients with advanced solid tumours, British journal of cancer 122(11) (2020) 1630-1637.
588 [24] C. Hoff, P. Seranski, J. Mollenhauer, B. Korn, T. Detzel, R. Reinhardt, J. Ramser, A. Poustka,
589 Physical and transcriptional mapping of the 17p13.3 region that is frequently deleted in human cancer,
590 Genomics 70(1) (2000) 26-33.
591 [25] J.D. McDonald, L. Daneshvar, J.R. Willert, K. Matsumura, F. Waldman, P.H. Cogen, Physical
592 mapping of chromosome 17p13.3 in the region of a putative tumor suppressor gene important in
593 medulloblastoma, Genomics 23(1) (1994) 229-32.
594 [26] E. Steichen-Gersdorf, M. Baumgartner, A. Kreczy, H. Maier, F.M. Fink, Deletion mapping on
595 chromosome 17p in medulloblastoma, British journal of cancer 76(10) (1997) 1284-7.

[27] R.K. Kanchan, N. Perumal, P. Atri, R. Chirravuri Venkata, I. Thapa, D.L. Klinkebiel, A.M. Donson, D. Perry, M. Punsoni, G.A. Talmon, D.W. Coulter, D.R. Boue, M. Snuderl, M.W. Nasser, S.K. Batra, R. Vibhakar, S. Mahapatra, MiR-1253 exerts tumor-suppressive effects in medulloblastoma via inhibition of CDK6 and CD276 (B7-H3), Brain Pathol 30(4) (2020) 732-745.

[28] N. Perumal, R.K. Kanchan, D. Doss, N. Bastola, P. Atri, R. Chirravuri-Venkata, I. Thapa, R. Vengoji, S.K. Maurya, D. Klinkebiel, G.A. Talmon, M.W. Nasser, S.K. Batra, S. Mahapatra, MiR-212-3p functions as a tumor suppressor gene in group 3 medulloblastoma via targeting nuclear factor I/B (NFIB), Acta neuropathologica communications 9(1) (2021).

[29] Y. Mao, W. Li, K. Chen, Y. Xie, Q. Liu, M. Yao, W. Duan, X. Zhou, R. Liang, M. Tao, B7-H1 and B7-H3 are independent predictors of poor prognosis in patients with non-small cell lung cancer, Oncotarget 6(5) (2015) 3452-61.

[30] F.B. Kang, L. Wang, H.C. Jia, D. Li, H.J. Li, Y.G. Zhang, D.X. Sun, B7-H3 promotes aggression and invasion of hepatocellular carcinoma by targeting epithelial-to-mesenchymal transition via JAK2/STAT3/Slug signaling pathway, Cancer Cell Int 15 (2015) 45.

[31] M. Liu, Y. Zhang, J. Zhang, H. Cai, C. Zhang, Z. Yang, Y. Niu, H. Wang, X. Wei, W. Wang, P. Gao, H. Li, J. Zhang, G. Sun, MicroRNA-1253 suppresses cell proliferation and invasion of non-small-cell lung carcinoma by targeting WNT5A, Cell death & disease 9(2) (2018) 189.

[32] J. Mo, T. Zheng, L. Lei, P. Dai, J. Liu, H. He, J. Shi, X. Chen, T. Guo, B. Yuan, G. Ji, MicroRNA-1253 Suppresses Cell Proliferation Migration and Invasion of Osteosarcoma by Targeting MMP9, Technol Cancer Res Treat 20 (2021) 1533033821995278.

[33] Y. Xu, Y. Yao, P. Gao, Y. Cui, Upregulated circular RNA circ_0030235 predicts unfavorable prognosis in pancreatic ductal adenocarcinoma and facilitates cell progression by sponging miR-1253 and miR-1294, Biochem Biophys Res Commun 509(1) (2019) 138-142.

[34] M.J. Merino, S. Gil, C.G. Macias, K. Lara, The Unknown microRNA Expression of Male Breast Cancer. Similarities and Differences with Female Ductal Carcinoma. Their Role as Tumor Biomarker, Journal of Cancer 9(3) (2018) 450-459.

622 [35] D. Yang, D. Zhang, miR-1253, a novel tumor suppressor gene in colon cancer, is associated with
623 poor patients prognosis, Clin Exp Med (2021).
624 [36] G. Szakacs, J.K. Paterson, J.A. Ludwig, C. Booth-Genthe, M.M. Gottesman, Targeting multidrug
625 resistance in cancer, Nature reviews. Drug discovery 5(3) (2006) 219-34.
626 [37] Y.H. Choi, A.M. Yu, ABC transporters in multidrug resistance and pharmacokinetics, and strategies
627 for drug development, Current pharmaceutical design 20(5) (2014) 793-807.
628 [38] L. Bao, S. Hazari, S. Mehra, D. Kaushal, K. Moroz, S. Dash, Increased expression of P-glycoprotein
629 and doxorubicin chemoresistance of metastatic breast cancer is regulated by miR-298, The American
630 journal of pathology 180(6) (2012) 2490-503.
631 [39] M. Morfouace, S. Cheepala, S. Jackson, Y. Fukuda, Y.T. Patel, S. Fatima, D. Kawauchi, A.A.
632 Shelat, C.F. Stewart, B.P. Sorrentino, J.D. Schuetz, M.F. Roussel, ABCG2 Transporter Expression
633 Impacts Group 3 Medulloblastoma Response to Chemotherapy, Cancer Res 75(18) (2015) 3879-89.
634 [40] N. Maio, K.S. Kim, G. Holmes-Hampton, A. Singh, T.A. Rouault, Dimeric ferrochelatase bridges
635 ABCB7 and ABCB10 homodimers in an architecturally defined molecular complex required for heme
636 biosynthesis, Haematologica 104(9) (2019) 1756-1767.
637 [41] J.Y. Kim, J.K. Kim, H. Kim, ABCB7 simultaneously regulates apoptotic and non-apoptotic cell
638 death by modulating mitochondrial ROS and HIF1alpha-driven NFkappaB signaling, Oncogene 39(9)
639 (2020) 1969-1982.
640 [42] B.R. Stockwell, J.P. Friedmann Angeli, H. Bayir, A.I. Bush, M. Conrad, S.J. Dixon, S. Fulda, S.
641 Gascon, S.K. Hatzios, V.E. Kagan, K. Noel, X. Jiang, A. Linkermann, M.E. Murphy, M. Overholtzer, A.
642 Oyagi, G.C. Pagnussat, J. Park, Q. Ran, C.S. Rosenfeld, K. Salnikow, D. Tang, F.M. Torti, S.V. Torti, S.
643 Toyokuni, K.A. Woerpel, D.D. Zhang, Ferroptosis: A Regulated Cell Death Nexus Linking Metabolism,
644 Redox Biology, and Disease, Cell 171(2) (2017) 273-285.
645 [43] J.P. Friedmann Angeli, M. Schneider, B. Proneth, Y.Y. Tyurina, V.A. Tyurin, V.J. Hammond, N.
646 Herbach, M. Aichler, A. Walch, E. Eggenhofer, D. Basavarajappa, O. Radmark, S. Kobayashi, T. Seibt,
647 H. Beck, F. Neff, I. Esposito, R. Wanke, H. Forster, O. Yefremova, M. Heinrichmeyer, G.W. Bornkamm,

E.K. Geissler, S.B. Thomas, B.R. Stockwell, V.B. O'Donnell, V.E. Kagan, J.A. Schick, M. Conrad, Inactivation of the ferroptosis regulator Gpx4 triggers acute renal failure in mice, Nat Cell Biol 16(12) (2014) 1180-91.

[44] T. Hirschhorn, B.R. Stockwell, The development of the concept of ferroptosis, Free Radic Biol Med 133 (2019) 130-143.

[45] J. Guo, B. Xu, Q. Han, H. Zhou, Y. Xia, C. Gong, X. Dai, Z. Li, G. Wu, Ferroptosis: A Novel Anti-tumor Action for Cisplatin, Cancer Res Treat 50(2) (2018) 445-460.

[46] L. Jiang, N. Kon, T. Li, S.J. Wang, T. Su, H. Hibshoosh, R. Baer, W. Gu, Ferroptosis as a p53-mediated activity during tumour suppression, Nature 520(7545) (2015) 57-62.

[47] X. Zhang, S. Sui, L. Wang, H. Li, L. Zhang, S. Xu, X. Zheng, Inhibition of tumor propellant glutathione peroxidase 4 induces ferroptosis in cancer cells and enhances anticancer effect of cisplatin, J Cell Physiol 235(4) (2020) 3425-3437.

[48] A. Drusco, A set of differentially expressed cerebro-spinal fluid (CSF) miRNAs can diagnose CNS malignancies, (2015).

[49] R.K. Kanchan, N. Perumal, P. Atri, R. Chirravuri Venkata, I. Thapa, D.L. Klinkebiel, A.M. Donson, D. Perry, M. Punsoni, G.A. Talmon, D.W. Coulter, D.R. Boue, M. Snuderl, M.W. Nasser, S.K. Batra, R. Vibhakar, S. Mahapatra, MiR-1253 exerts tumor-suppressive effects in medulloblastoma via inhibition of CDK6 and CD276 (B7-H3), Brain pathology (Zurich, Switzerland) (2020).

[50] H. Weishaupt, P. Johansson, A. Sundstrom, Z. Lubovac-Pilav, B. Olsson, S. Nelander, F.J. Swartling, Batch-normalization of cerebellar and medulloblastoma gene expression datasets utilizing empirically defined negative control genes, Bioinformatics 35(18) (2019) 3357-3364.

[51] J.B. Kaushal, R. Bhatia, R.K. Kanchan, P. Raut, S. Mallapragada, Q.P. Ly, S.K. Batra, S. Rachagani, Repurposing Niclosamide for Targeting Pancreatic Cancer by Inhibiting Hh/Gli Non-Canonical Axis of Gsk3beta, Cancers (Basel) 13(13) (2021).

[52] V. Srinivasan, A.J. Pierik, R. Lill, Crystal structures of nucleotide-free and glutathione-bound mitochondrial ABC transporter Atm1, Science 343(6175) (2014) 1137-40.

[53] C. Pondarre, B.B. Antiochos, D.R. Campagna, S.L. Clarke, E.L. Greer, K.M. Deck, A. McDonald, A.P. Han, A. Medlock, J.L. Kutok, S.A. Anderson, R.S. Eisenstein, M.D. Fleming, The mitochondrial ATP-binding cassette transporter Abcb7 is essential in mice and participates in cytosolic iron-sulfur cluster biogenesis, Hum Mol Genet 15(6) (2006) 953-64.

[54] A. Seguin, D.M. Ward, Mitochondrial ABC Transporters and Iron Metabolism, Journal of Clinical & Experimental Pathology 08(01) (2018).

[55] Y. Zhao, J. Li, W. Guo, H. Li, L. Lei, Periodontitis-level butyrate-induced ferroptosis in periodontal ligament fibroblasts by activation of ferritinophagy, Cell Death Discov 6(1) (2020) 119.

[56] T. Tadokoro, M. Ikeda, T. Ide, H. Deguchi, S. Ikeda, K. Okabe, A. Ishikita, S. Matsushima, T. Koumura, K.I. Yamada, H. Imai, H. Tsutsui, Mitochondria-dependent ferroptosis plays a pivotal role in doxorubicin cardiotoxicity, JCI Insight 5(9) (2020).

[57] S. Dev, J.L. Babitt, Overview of iron metabolism in health and disease, Hemodial Int 21 Suppl 1 (2017) S6-S20.

[58] H. Li, Y. Liu, L. Shang, J. Cai, J. Wu, W. Zhang, X. Pu, W. Dong, T. Qiao, K. Li, Iron regulatory protein 2 modulates the switch from aerobic glycolysis to oxidative phosphorylation in mouse embryonic fibroblasts, Proc Natl Acad Sci U S A 116(20) (2019) 9871-9876.

[59] R.J. Mailloux, Mitochondrial Antioxidants and the Maintenance of Cellular Hydrogen Peroxide Levels, Oxid Med Cell Longev 2018 (2018) 7857251.

[60] R.C. Hider, X.L. Kong, Glutathione: a key component of the cytoplasmic labile iron pool, Biometals 24(6) (2011) 1179-87.

[61] B. Hassannia, B. Wiernicki, I. Ingold, F. Qu, S. Van Herck, Y.Y. Tyurina, H. Bayir, B.A. Abhari, J.P.F. Angeli, S.M. Choi, E. Meul, K. Heyninck, K. Declerck, C.S. Chirumamilla, M. Lahtela-Kakkonen, G. Van Camp, D.V. Krysko, P.G. Ekert, S. Fulda, B.G. De Geest, M. Conrad, V.E. Kagan, W. Vanden Berghe, P. Vandenabeele, T. Vanden Berghe, Nano-targeted induction of dual ferroptotic mechanisms eradicates high-risk neuroblastoma, J Clin Invest 128(8) (2018) 3341-3355.

699 [62] S. Dasari, P.B. Tchounwou, Cisplatin in cancer therapy: molecular mechanisms of action, Eur J
700 Pharmacol 740 (2014) 364-78.
701 [63] Y. Zhou, Y. Shen, C. Chen, X. Sui, J. Yang, L. Wang, J. Zhou, The crosstalk between autophagy and
702 ferroptosis: what can we learn to target drug resistance in cancer?, Cancer Biol Med 16(4) (2019) 630-
703 646.
704 [64] M. Berndtsson, M. Hagg, T. Panaretakis, A.M. Havelka, M.C. Shoshan, S. Linder, Acute apoptosis
705 by cisplatin requires induction of reactive oxygen species but is not associated with damage to nuclear
706 DNA, International journal of cancer. Journal international du cancer 120(1) (2007) 175-80.
707 [65] R. Gilbertson, C. Wickramasinghe, R. Hernan, V. Balaji, D. Hunt, D. Jones-Wallace, J. Crolla, R.
708 Perry, J. Lunec, A. Pearson, D. Ellison, Clinical and molecular stratification of disease risk in
709 medulloblastoma, British journal of cancer 85(5) (2001) 705-12.
710 [66] N.G. Gottardo, J.R. Hansford, J.P. McGlade, F. Alvaro, D.M. Ashley, S. Bailey, D.L. Baker, F.
711 Bourdeaut, Y.J. Cho, M. Clay, S.C. Clifford, R.J. Cohn, C.H. Cole, P.B. Dallas, P. Downie, F. Doz, D.W.
712 Ellison, R. Endersby, P.G. Fisher, T. Hassall, J.A. Heath, H.L. Hii, D.T. Jones, R. Junckerstorff, S. Kellie,
713 M. Kool, R.S. Kotecha, P. Lichter, S.J. Laughton, S. Lee, G. McCowage, P.A. Northcott, J.M. Olson, R.J.
714 Packer, S.M. Pfister, T. Pietsch, B. Pizer, S.L. Pomeroy, M. Remke, G.W. Robinson, S. Rutkowski, T.
715 Schoep, A.A. Shelat, C.F. Stewart, M. Sullivan, M.D. Taylor, B. Wainwright, T. Walwyn, W.A. Weiss,
716 D. Williamson, A. Gajjar, Medulloblastoma Down Under 2013: a report from the third annual meeting of
717 the International Medulloblastoma Working Group, Acta neuropathologica 127(2) (2014) 189-201.
718 [67] Y.J. Cho, A. Tsherniak, P. Tamayo, S. Santagata, A. Ligon, H. Greulich, R. Berhoukim, V. Amani,
719 L. Goumnerova, C.G. Eberhart, C.C. Lau, J.M. Olson, R.J. Gilbertson, A. Gajjar, O. Delattre, M. Kool, K.
720 Ligon, M. Meyerson, J.P. Mesirov, S.L. Pomeroy, Integrative genomic analysis of medulloblastoma
721 identifies a molecular subgroup that drives poor clinical outcome, Journal of clinical oncology : official
722 journal of the American Society of Clinical Oncology 29(11) (2011) 1424-30.
723 [68] P. Tamayo, Y.J. Cho, A. Tsherniak, H. Greulich, L. Ambrogio, N. Schouten-van Meeteren, T. Zhou,
724 A. Buxton, M. Kool, M. Meyerson, S.L. Pomeroy, J.P. Mesirov, Predicting relapse in patients with

725 medulloblastoma by integrating evidence from clinical and genomic features, Journal of clinical oncology
726 : official journal of the American Society of Clinical Oncology 29(11) (2011) 1415-23.
727 [69] E.M. Thompson, T. Hielscher, E. Bouffet, M. Remke, B. Luu, S. Gururangan, R.E. McLendon, D.D.
728 Bigner, E.S. Lipp, S. Perreault, Y.-J. Cho, G. Grant, S.-K. Kim, J.Y. Lee, A.A.N. Rao, C. Giannini,
729 K.K.W. Li, H.-K. Ng, Y. Yao, T. Kumabe, T. Tominaga, W.A. Grajkowska, M. Perek-Polnik, D.C.Y.
730 Low, W.T. Seow, K.T.E. Chang, J. Mora, I.F. Pollack, R.L. Hamilton, S. Leary, A.S. Moore, W.J.
731 Ingram, A.R. Hallahan, A. Jouvet, M. Fèvre-Montange, A. Vasiljevic, C. Faure-Conter, T. Shofuda, N.
732 Kagawa, N. Hashimoto, N. Jabado, A.G. Weil, T. Gayden, T. Wataya, T. Shalaby, M. Grotzer, K.
733 Zitterbart, J. Sterba, L. Kren, T. Hortobágyi, A. Klekner, B. László, T. Pócza, P. Hauser, U. Schüller, S.
734 Jung, W.-Y. Jang, P.J. French, J.M. Kros, M.-L.C. van Veelen, L. Massimi, J.R. Leonard, J.B. Rubin, R.
735 Vibhakar, L.B. Chambless, M.K. Cooper, R.C. Thompson, C.C. Faria, A. Carvalho, S. Nunes, J.
736 Pimentel, X. Fan, K.M. Muraszko, E. López-Aguilar, D. Lyden, L. Garzia, D.J.H. Shih, N. Kijima, C.
737 Schneider, J. Adamski, P.A. Northcott, M. Kool, D.T.W. Jones, J.A. Chan, A. Nikolic, M.L. Garre, E.G.
738 Van Meir, S. Osuka, J.J. Olson, A. Jahangiri, B.A. Castro, N. Gupta, W.A. Weiss, I. Moxon-Emre, D.J.
739 Mabbott, A. Lassaletta, C.E. Hawkins, U. Tabori, J. Drake, A. Kulkarni, P. Dirks, J.T. Rutka, A.
740 Korshunov, S.M. Pfister, R.J. Packer, V. Ramaswamy, M.D. Taylor, Prognostic value of
741 medulloblastoma extent of resection after accounting for molecular subgroup: a retrospective integrated
742 clinical and molecular analysis, The Lancet Oncology 17(4) (2016) 484-495.
743 [70] O. Menyhart, F. Giangaspero, B. Gyorffy, Molecular markers and potential therapeutic targets in
744 non-WNT/non-SHH (group 3 and group 4) medulloblastomas, J Hematol Oncol 12(1) (2019) 29.
745 [71] E. Ward, C. DeSantis, A. Robbins, B. Kohler, A. Jemal, Childhood and adolescent cancer statistics,
746 2014, CA Cancer J Clin 64(2) (2014) 83-103.
747 [72] R.M. Hill, S. Richardson, E.C. Schwalbe, D. Hicks, J.C. Lindsey, S. Crosier, G. Rafiee, Y.
748 Grabovska, S.B. Wharton, T.S. Jacques, A. Michalski, A. Joshi, B. Pizer, D. Williamson, S. Bailey, S.C.
749 Clifford, Time, pattern, and outcome of medulloblastoma relapse and their association with tumour

biology at diagnosis and therapy: a multicentre cohort study, The Lancet Child & Adolescent Health 4(12) (2020) 865-874.

[73] K.V. Hoff, B. Hinkes, N.U. Gerber, F. Deinlein, U. Mittler, C. Urban, M. Benesch, M. Warmuth-Metz, N. Soerensen, I. Zwiener, H. Goette, P.G. Schlegel, T. Pietsch, R.D. Kortmann, J. Kuehl, S. Rutkowski, Long-term outcome and clinical prognostic factors in children with medulloblastoma treated in the prospective randomised multicentre trial HIT'91, Eur J Cancer 45(7) (2009) 1209-1217.

[74] K. Ribi, C. Relly, M.A. Landolt, F.D. Alber, E. Boltshauser, M.A. Grotzer, Outcome of medulloblastoma in children: long-term complications and quality of life, Neuropediatrics 36(6) (2005) 357-65.

[75] R.T. Othman, I. Kimishi, T.D. Bradshaw, L.C. Storer, A. Korshunov, S.M. Pfister, R.G. Grundy, I.D. Kerr, B. Coyle, Overcoming multiple drug resistance mechanisms in medulloblastoma, Acta Neuropathol Commun 2 (2014) 57.

[76] P.M. Chou, M. Reyes-Mugica, N. Barquin, T. Yasuda, X. Tan, T. Tomita, Multidrug resistance gene expression in childhood medulloblastoma: correlation with clinical outcome and DNA ploidy in 29 patients, Pediatric neurosurgery 23(6) (1995) 283-91; discussion 291-2.

[77] S. Miroshnichenko, O. Patutina, Enhanced Inhibition of Tumorigenesis Using Combinations of miRNA-Targeted Therapeutics, Front Pharmacol 10 (2019) 488.

[78] P. Cavadini, G. Biasiotto, M. Poli, S. Levi, R. Verardi, I. Zanella, M. Derosas, R. Ingrassia, M. Corrado, P. Arosio, RNA silencing of the mitochondrial ABCB7 transporter in HeLa cells causes an iron-deficient phenotype with mitochondrial iron overload, Blood 109(8) (2007) 3552-9.

[79] A. Miyake, S. Higashijima, D. Kobayashi, T. Narita, T. Jindo, D.H. Setiamarga, S. Ohisa, N. Orihara, K. Hibiya, S. Konno, S. Sakaguchi, K. Horie, Y. Imai, K. Naruse, A. Kudo, H. Takeda, Mutation in the abcb7 gene causes abnormal iron and fatty acid metabolism in developing medaka fish, Dev Growth Differ 50(9) (2008) 703-16.

774 [80] P. Gonzalez-Cabo, A. Bolinches-Amoros, J. Cabello, S. Ros, S. Moreno, H.A. Baylis, F. Palau, R.P.
775 Vazquez-Manrique, Disruption of the ATP-binding cassette B7 (ABTM-1/ABCB7) induces oxidative
776 stress and premature cell death in Caenorhabditis elegans, J Biol Chem 286(24) (2011) 21304-14.
777 [81] V. Kumar, A.K. A, R. Sanawar, A. Jaleel, T.R. Santhosh Kumar, C.C. Kartha, Chronic Pressure
778 Overload Results in Deficiency of Mitochondrial Membrane Transporter ABCB7 Which Contributes to
779 Iron Overload, Mitochondrial Dysfunction, Metabolic Shift and Worsens Cardiac Function, Sci Rep 9(1)
780 (2019) 13170.
781 [82] M.T. Nunez, C. Nunez-Millacura, V. Tapia, P. Munoz, D. Mazariegos, M. Arredondo, P. Munoz, C.
782 Mura, R.B. Maccioni, Iron-activated iron uptake: a positive feedback loop mediated by iron regulatory
783 protein 1, Biometals 16(1) (2003) 83-90.
784 [83] S.J. Dixon, B.R. Stockwell, The role of iron and reactive oxygen species in cell death, Nat Chem
785 Biol 10(1) (2014) 9-17.
786 [84] Y. Mou, J. Wang, J. Wu, D. He, C. Zhang, C. Duan, B. Li, Ferroptosis, a new form of cell death:
787 opportunities and challenges in cancer, J Hematol Oncol 12(1) (2019) 34.
788 [85] M. Abdalkader, R. Lampinen, K.M. Kanninen, T.M. Malm, J.R. Liddell, Targeting Nrf2 to Suppress
789 Ferroptosis and Mitochondrial Dysfunction in Neurodegeneration, Front Neurosci 12 (2018) 466.
790 [86] N.S. Aboelella, C. Brandle, T. Kim, Z.C. Ding, G. Zhou, Oxidative Stress in the Tumor
791 Microenvironment and Its Relevance to Cancer Immunotherapy, Cancers (Basel) 13(5) (2021).
792 [87] W.S. Yang, R. SriRamaratnam, M.E. Welsch, K. Shimada, R. Skouta, V.S. Viswanathan, J.H.
793 Cheah, P.A. Clemons, A.F. Shamji, C.B. Clish, L.M. Brown, A.W. Girotti, V.W. Cornish, S.L. Schreiber,
794 B.R. Stockwell, Regulation of ferroptotic cancer cell death by GPX4, Cell 156(1-2) (2014) 317-331.
795 [88] M.M. Gaschler, A.A. Andia, H. Liu, J.M. Csuka, B. Hurlocker, C.A. Vaiana, D.W. Heindel, D.S.
796 Zuckerman, P.H. Bos, E. Reznik, L.F. Ye, Y.Y. Tyurina, A.J. Lin, M.S. Shchepinov, A.Y. Chan, E.
797 Peguero-Pereira, M.A. Fomich, J.D. Daniels, A.V. Bekish, V.V. Shmanai, V.E. Kagan, L.K. Mahal, K.A.
798 Woerpel, B.R. Stockwell, FINO2 initiates ferroptosis through GPX4 inactivation and iron oxidation, Nat
799 Chem Biol 14(5) (2018) 507-515.

[89] P. Fan, L. Liu, Y. Yin, Z. Zhao, Y. Zhang, P.S. Amponsah, X. Xiao, N. Bauer, A. Abukiwan, C.C. Nwaeburu, J. Gladkich, C. Gao, P. Schemmer, W. Gross, I. Herr, MicroRNA-101-3p reverses gemcitabine resistance by inhibition of ribonucleotide reductase M1 in pancreatic cancer, Cancer Lett 373(1) (2016) 130-137.

[90] G. Yu, B. Jia, Y. Cheng, L. Zhou, B. Qian, Z. Liu, Y. Wang, MicroRNA-429 sensitizes pancreatic cancer cells to gemcitabine through regulation of PDCD4, Am J Transl Res 9(11) (2017) 5048-5055.

[91] H. Chen, L. Liu, X. Li, Y. Shi, N. Liu, MicroRNA-1294 inhibits the proliferation and enhances the chemosensitivity of glioma to temozolomide via the direct targeting of TPX2, Am J Cancer Res 8(2) (2018) 291-301.

[92] J. Jiang, C. Xie, Y. Liu, Q. Shi, Y. Chen, Up-regulation of miR-383-5p suppresses proliferation and enhances chemosensitivity in ovarian cancer cells by targeting TRIM27, Biomed Pharmacother 109 (2019) 595-601.

[93] M.J. Tu, P.Y. Ho, Q.Y. Zhang, C. Jian, J.X. Qiu, E.J. Kim, R.J. Bold, F.J. Gonzalez, H. Bi, A.M. Yu, Bioengineered miRNA-1291 prodrug therapy in pancreatic cancer cells and patient-derived xenograft mouse models, Cancer Lett 442 (2019) 82-90.

[94] M. Wang, R. Qiu, S. Yu, X. Xu, G. Li, R. Gu, C. Tan, W. Zhu, B. Shen, Paclitaxelresistant gastric cancer MGC803 cells promote epithelialtomesenchymal transition and chemoresistance in paclitaxelsensitive cells via exosomal delivery of miR1555p, Int J Oncol 54(1) (2019) 326-338.

[95] V.B. Konkimalla, B. Kaina, T. Efferth, Role of transporter genes in cisplatin resistance, In Vivo 22(3) (2008) 279-83.

Figure Legends

Figure 1. ABCB7, a target of miR-1253, is deregulated in group 3 MB. (A) Subgroup-specific ABCB7 expression assessment by RNA sequencing (log_2 transcripts per million) of a local medulloblastoma patient cohort (Kanchan *et al.*, GSE) showing specific deregulation in group 3 tumors. *CB*, pediatric cerebellum (n=10); *SHH*, sonic hedgehog (n=6); *G3*, group 3 (n=7); *G4*, group 4 (n=12). **(B)** Poor prognostic profile demonstrable in high-expressing group 3 MB patients (Cavali *et al.* GSE85217). **(C)** Confocal microscopic images confirming high ABCB7 expression in group 3 MB tumors (n=6) compared to pediatric cerebellum (n=6) and colocalization to the mitochondria based on COXIV fluorescence. Images captured at 10X magnification. **(D)** Western blotting analysis showing high ABCB7 expression in classic MB cell lines (group 3: D341, D425, HDMB03, D556; group 3/4: D283) compared to normal human astrocytes (NHA). Western blotting analysis showing downregulation of ABCB7 with miR-1253 overexpression in **(E)** D425 and **(F)** HDMB03 cells. **(G)** Confocal microscopic images in D425 and HDMB03 cells showing co-localization of ABCB7 to the mitochondria and downregulation with miR-1253 overexpression. Images captured at 63X magnification. **(H)** Dual-luciferase assay confirming direct binding of miR-1253 to ABCB7 in HDMB03 cells. Data presented as mean ± SD from experiments done in triplicates and analyzed using Mann-Whitney U test (**A**) or Student's t-test **(H)** (*p <0.05, **p <0.01, ***p <0.001, ****p <0.0001).

Figure 2. MiR-1253 triggers iron imbalance in group 3 MB cells. Confocal images showing Calcein AM dye quenching in miR-1253-transfected **(A)** D425 and **(B)** HDMB03 cells indicating high cytosolic labile iron compared to scramble (NC) transfected cells. Fe^{2+} stained with Calcein AM (**green**), and nuclei stained with DAPI (**blue**). Similarly, escalation in both **(C)** cytosolic and **(D)** mitochondrial free Fe^{2+} demonstrable with miR-1253 expression, abrogated by

iron chelation with DFO. Mitochondria stained with MitoTracker™ Deep Red FM (**red**); cytosolic Fe^{2+} stained with FerroOrange (**orange**); mitochondrial Fe^{2+} stained with Mito-FerroGreen (**green**). Images captured at 63X.

Figure 3. MiR-1253 triggers oxidative stress and lipid peroxidation leading to cell death in group 3 MB cells. Confocal images showing elevated mitochondrial $O_2^{\bullet -}$ (MitoSOX™ Red, **red**) and cytosolic H_2O_2 (DCFDA, **green**) following miR-1253 expression in **(A)** D425 and **(B)** HDMB03 cells. Higher lipid peroxidation (measured by Image-iT® Lipid Peroxidation Kit) also noted in miR-1253 transfected **(C)** D425 and **(D)** HDMB03 cells. Flow cytometry analysis showing significantly higher $O_2^{\bullet -}$ mediated cell death (representing ferroptosis) in miR-1253-expressing **(E)** D425 and **(F)** HDMB03 cells demonstrable by quantifying cells staining for both Annexin V-Cy5 (apoptosis) and for $O_2^{\bullet -}$ (Mitosox) (Q2). Data presented as mean ± SD from experiments done in triplicates and analyzed using Student's t-test (**p* <0.05, ***p* <0.01, ****p* <0.001, *****p* <0.0001). Images captured either at 20X (**A** and **B**) or 63X (**C** and **D**) magnification. Scale bar 200 µm.

Figure 4. $ABCB7^{KO}$ can trigger iron imbalance and oxidative stress in group 3 MB cells. CRISPR/Cas9-mediated ABCB7 gene knockout in HDMB03 cells confirmed by **(A)** RT-PCR and **(B)** Western blotting. **(C)** Confocal images showing Calcein AM dye quenching in $ABCB7^{KO}$ HDMB03 cells suggestive of high cytosolic labile iron compared to wild-type (WT) cells. Fe^{2+} stained with Calcein AM (**green**) and nuclei stained with DAPI (**blue**). Confocal images demonstrating escalation in both **(D)** cytosolic and **(E)** mitochondrial free Fe^{2+} with ABCB7 knockout, abrogated by iron chelation with DFO. Mitochondria stained with MitoTracker™ Deep Red FM (**red**); cytosolic Fe^{2+} stained with FerroOrange (**orange**); mitochondrial Fe^{2+} stained with Mito-FerroGreen (**green**). **(F)** Elevated oxidative stress

demonstrable in ABCB7^{KO} HDMB03 cells as evidenced by higher mitochondrial $O_2^{\bullet -}$ (MitoSOX™ Red, **red**) and cytosolic H_2O_2 (DCFDA, **green**) compared to wild-type. Images captured at 63X (**C-E**) or 20X (**F**) magnification. Scale bar 400 µm. Data presented as mean ± SD from experiments done in triplicates and analyzed using Student's t-test (*p <0.05, **p <0.01, ***p <0.001, ****p <0.0001).

Figure 5. MiR-1253 and ABCB7 regulate GPX4 expression, a key regulator of ferroptosis. **(A)** Schematic showing the important role of GPX4 in mitigating ferroptosis. Image created with Biorender.com. **(B)** Subgroup-specific GPX4 expression assessment by RNA sequencing (log_2 transcripts per million) of a local medulloblastoma patient cohort (Kanchan *et al.*, GSE148390) showing deregulation in MB tumors, highest in group 3 MB. *CB*, pediatric cerebellum (n=10); *SHH*, sonic hedgehog (n=6); *G3*, group 3 (n=7); *G4*, group 4 (n=12). **(C)** Poor prognostic profile demonstrable in high-expressing MB patients (Cavali *et al*. GSE85217). **(D)** Confocal microscopic images confirming high GPX4 expression in group 3 MB tumors (n=6) compared to pediatric cerebellum (n=6) and colocalization to the mitochondria based on COXIV fluorescence. Images captured at 10X magnification. **(E)** Western blotting analysis showing high *in vitro* GPX4 expression in classic MB cell lines (group 3: D341, D425, HDMB03; group 3/4: D283) compared to normal human astrocytes (NHA). **(F)** Western blotting analysis showing a strong inhibitory effect of miR-1253 on GPX4 expression in D425 and HDMB03 cells. **(G)** Near-abrogation of GPX4 expression with ABCB7 knockout in HDMB03 cells. Spearman correlation showing positive correlation between ABCB7 and GPX4 expression. (Kanchan *et al.*, GSE148390). **(H)** Similar inhibitory effect noted on total glutathione (GSH) levels in miR-1253-transfected D425 and HDMB03 cells. Data presented as mean ± SD from experiments done in triplicates and analyzed using Student's t-test (*p <0.05, **p <0.01, ***p <0.001).

Figure 6. MiR-1253 potentiates cisplatin toxicity in group 3 MB cells. IC_{50} of cisplatin in **(A)** D425 and **(B)** HDMB03 cells transfected with scramble vs. miR-1253 for 24-72 h. **(C)** Tabulated results presented as fold-change in cisplatin IC_{50} between scramble and miR-1253 in D425 and HDMB03 cells at different time points. **(D)** Colonogenic assay demonstrating inhibitory effect of cisplatin vs. miR-1253 vs. combination on colony formation in HDMB03 cells. MiR-1253-transfected **(E)** D425 and **(F)** HDMB03, and **(G)** $ABCB7^{KO}$ HDMB03 cells treated with cisplatin (D425 24-h IC_{25} ~10 µM; HDMB03 24-h IC_{25} ~2 µM) and stained with MitoSOX™ Red (**red**) for mitochondrial superoxide anions ($O_2^{\bullet -}$) and DCFDA (**green**) for cytosolic ROS (H_2O_2). Representative images and graphs showing the potentiating effect of combining miR-1253 with cisplatin. Images captured at 20X magnification. Scale bar 400 µm. Data presented as mean ± SD from experiments done in triplicates and analyzed using one-way analysis of variance (**p* <0.05, ***p* <0.01, ****p* <0.001, *****p* <0.0001).

Figure 7. MiR-1253 potentiates cisplatin cytotoxicity in group 3 MB cells by ferroptosis. Oxidative stress measured by quantifying **(A)** mitochondrial $O_2^{\bullet -}$ (MitoSOX™ Red, **red**) and **(B)** cytosolic H_2O_2 (DCFDA, **green**) in miR-1253-transfected HDMB03 cells showing potentiating effect of miR-1253 on cisplatin, and inhibited by a ferroptosis inhibitor, ferrostatin-1 (FER). Images captured at 20X magnification. Scale bar 200 µm. **(C)** As measured by Image-iT® Lipid Peroxidation Kit, confocal images showing the highest lipid peroxidation in combination treatment groups (miR + Cis), again rescued by ferrostatin-1, in miR-1253-transfected HDMB03 cells. Images captured at 63X magnification. **(D)** Evaluation of oxidized glutathione (GSH) showing punctuated effects in combination treatment groups (miR + Cis) with rescue in the presence of ferrostatin in miR-1253-transfected HDMB03 cells. **(E)** Analysis of cell death by flow cytometry showing significantly higher $O_2^{\bullet -}$ mediated cell death (representing

914 ferroptosis) in miR-1253-expressing HDMB03 cells demonstrable by quantifying cells staining
915 for both Annexin V-Cy5 (apoptosis) and for $O_2^{\bullet -}$ (Mitosox) (Q2). Data presented as mean ± SD
916 from experiments done in triplicates and analyzed using one-way analysis of variance (*p <0.05,
917 **p <0.01, ***p <0.001, ****p <0.0001).

918 **Supplementary Figure 1. Deregulated expression of ABCB7 in MB is associated with poor**
919 **survival and is negatively regulated by miR-1253. (A)** Enrichment plot by KEGG pathways
920 analysis demonstrating a strong negative enrichment score for the ABC transporter family with
921 miR-1253 expression restoration in HDMB03 cells. **(B)** ABC transporter expression heatmap
922 illustrating effect of miR-1253 overexpression in HDMB03 cells (by transient transfection). **(C)**
923 Deregulated ABC transporters in group 3 MB (column 1), effect of deregulated expression on
924 survival (column 2), and transporters significantly downregulated by miR-1253 expression
925 (column 3). This analysis revealed ABCB7 as the best putative target for miR-1253. **(D)**
926 Expression profile for ABCB7 in multiple MB cohorts. *CB*, normal cerebellum, Roth *et al.* 2008
927 (n=9, GSE3526); *MB 1*, Gilbertson *et al.* 2012 (n=76, GSE37418); *MB 2*, Pfister *et al.* 2017
928 (n=223); *MB 3*, Delattre *et al.* 2012 (n=57); *MB 4*, Kool *et al.* 2009 (n=62, GSE10327). **(E)** Poor
929 prognostic profile demonstrable in high ABCB7-expressing medulloblastoma patients (Cavali *et*
930 *al*. GSE85217). Subgroup-specific ABCB7 expression in two separate medulloblastoma patient
931 cohorts, i.e. **(F)** Weishaupt *et al.*, GSE124814; *CB*, normal cerebellum (n=291); *WNT*, wingless
932 (n=118); *SHH*, sonic hedgehog (n=405); *G3*, group 3 (n=233); *G4*, group 4 (n=530); and **(G)**
933 Luo *et al.*, GSE164677; *CB*, normal cerebellum (n=4); *WNT*, wingless (n=6); *SHH*, sonic
934 hedgehog (n=20); *G3*, group 3 (n=14); *G4*, group 4 (n=19); Data normalized via RUV method
935 **(F)** or DeSeq2 median of ratios (MoR) method **(G)** and both analyzed using Mann-Whitney U
936 (*p <0.05, **p <0.01, ***p <0.001, ****p <0.0001).

Supplementary Figure 2. GPX4 expression is elevated in medulloblastoma. Subgroup-specific GPX4 expression data from Weishaupt *et al.*, GSE124814; *CB*, normal cerebellum (n=291); *WNT*, wingless (n=118); *SHH*, sonic hedgehog (n=405); *G3*, group 3 (n=233); *G4*, group 4 (n=530); Data normalized via RUV method and analyzed using Mann-Whitney U (*p <0.05, **p <0.01, ***p <0.001, ****p <0.0001).

Supplementary Figure 3. ABCB7 knockout potentiates cisplatin cytotoxicity in group 3 MB cells by ferroptosis. Oxidative stress measured by quantifying **(A)** mitochondrial $O_2^{\bullet -}$ (MitoSOX™ Red, **red**) and **(B)** cytosolic H_2O_2 (DCFDA, **green**) in miR-1253-transfected HDMB03 cells showing potentiating effect of miR-1253 on cisplatin, and inhibited by a ferroptosis inhibitor, ferrostatin-1 (FER). Images captured at 20X magnification. Scale bar 200 µm. **(C)** As measured by Image-iT® Lipid Peroxidation Kit, confocal images showing the highest lipid peroxidation in combination treatment groups ($ABCB7^{KO}$ + Cis), again rescued by ferrostatin-1, in $ABCB7^{KO}$ HDMB03 cells. Images captured at 63X magnification. **(D)** Evaluation of oxidized glutathione (GSH) showing punctuated effects in combination treatment groups ($ABCB7^{KO}$ + Cis) with rescue in the presence of ferrostatin in $ABCB7^{KO}$ HDMB03 cells. Data presented as mean ± SD from experiments done in triplicates and analyzed using one-way analysis of variance (*p <0.05, **p <0.01, ***p <0.001, ****p <0.0001).

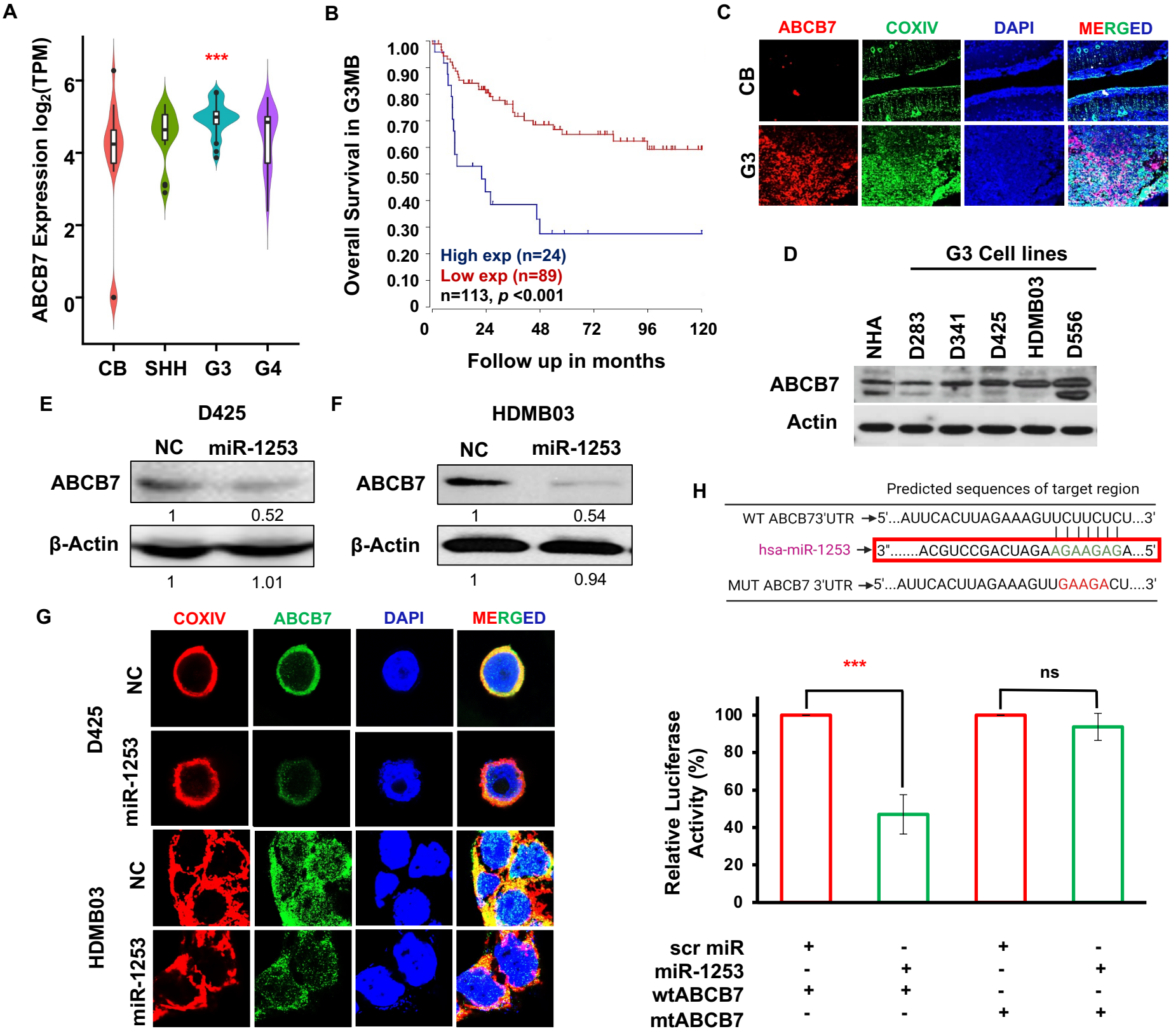
A
ABCB7 Expression log2(TPM)
***
CB
SHH
G3
G4
B
Overall Survival in G3MB
High exp (n=24)
Low exp (n=89)
n=113, p <0.001
Follow up in months
C
ABCB7
COXIV
DAPI
MERGED
CB
G3
D
G3 Cell lines
NHA
D283
D341
D425
HDMB03
D556
ABCB7
Actin
E
D425
NC
miR-1253
ABCB7
β-Actin
1
0.52
1
1.01
F
HDMB03
NC
miR-1253
ABCB7
β-Actin
1
0.54
1
0.94
G
COXIV
ABCB7
DAPI
MERGED
D425
NC
miR-1253
HDMB03
NC
miR-1253
H
Predicted sequences of target region
WT ABCB73'UTR →5'...AUUCACUUAGAAAGUUCUUCUCU...3'
hsa-miR-1253 →3".....ACGUCCGACUAGAAGAAGAGA...5'
MUT ABCB7 3'UTR →5'...AUUCACUUAGAAAGUUGAAGACU....3'
***
ns
Relative Luciferase Activity (%)
scr miR
miR-1253
wtABCB7
mtABCB7

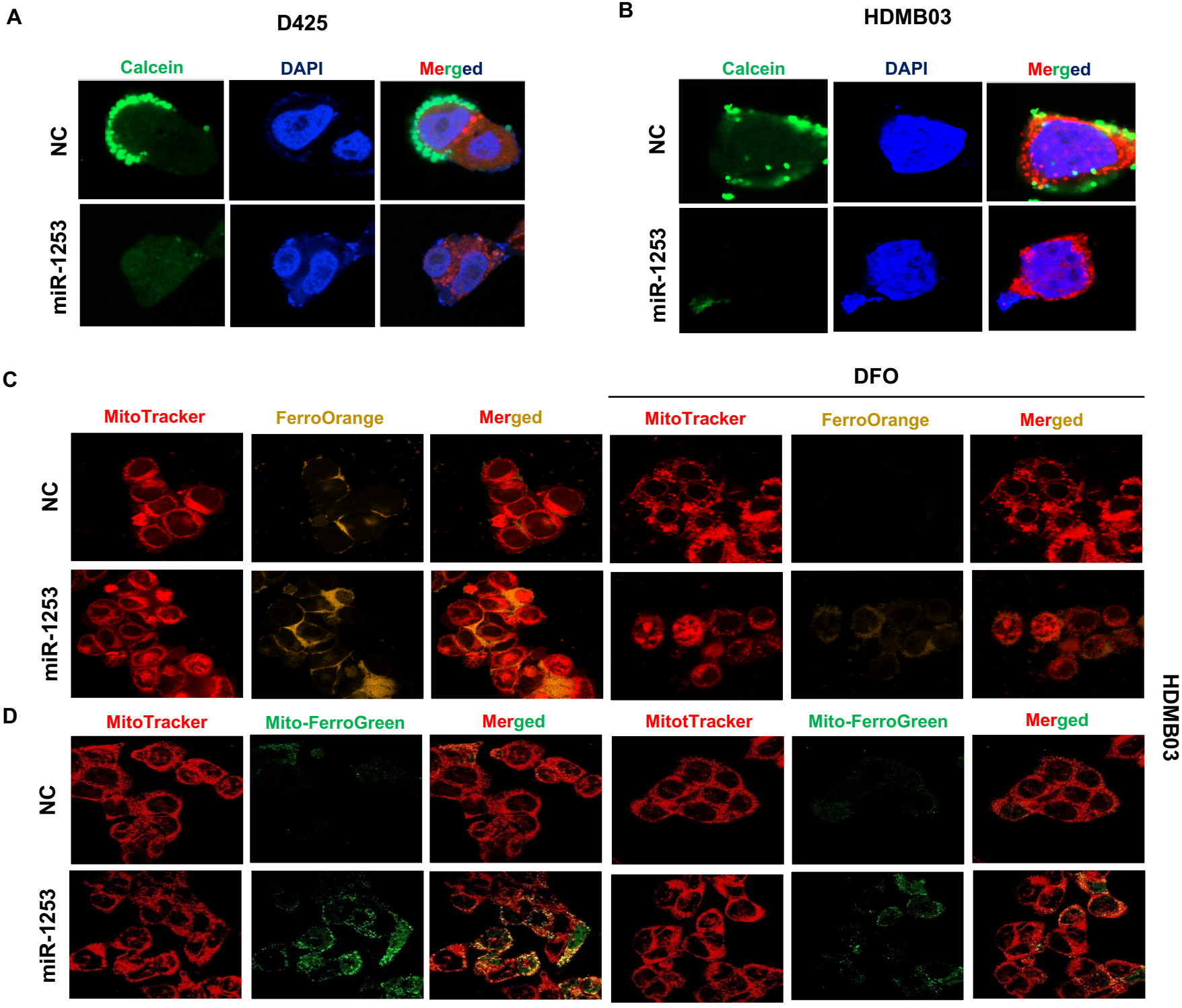
A
D425
Calcein
DAPI
Merged
NC
miR-1253
B
HDMB03
Calcein
DAPI
Merged
NC
miR-1253
C
DFO
MitoTracker
FerroOrange
Merged
MitoTracker
FerroOrange
Merged
NC
miR-1253
D
MitoTracker
Mito-FerroGreen
Merged
MitotTracker
Mito-FerroGreen
Merged
NC
miR-1253
HDMB03

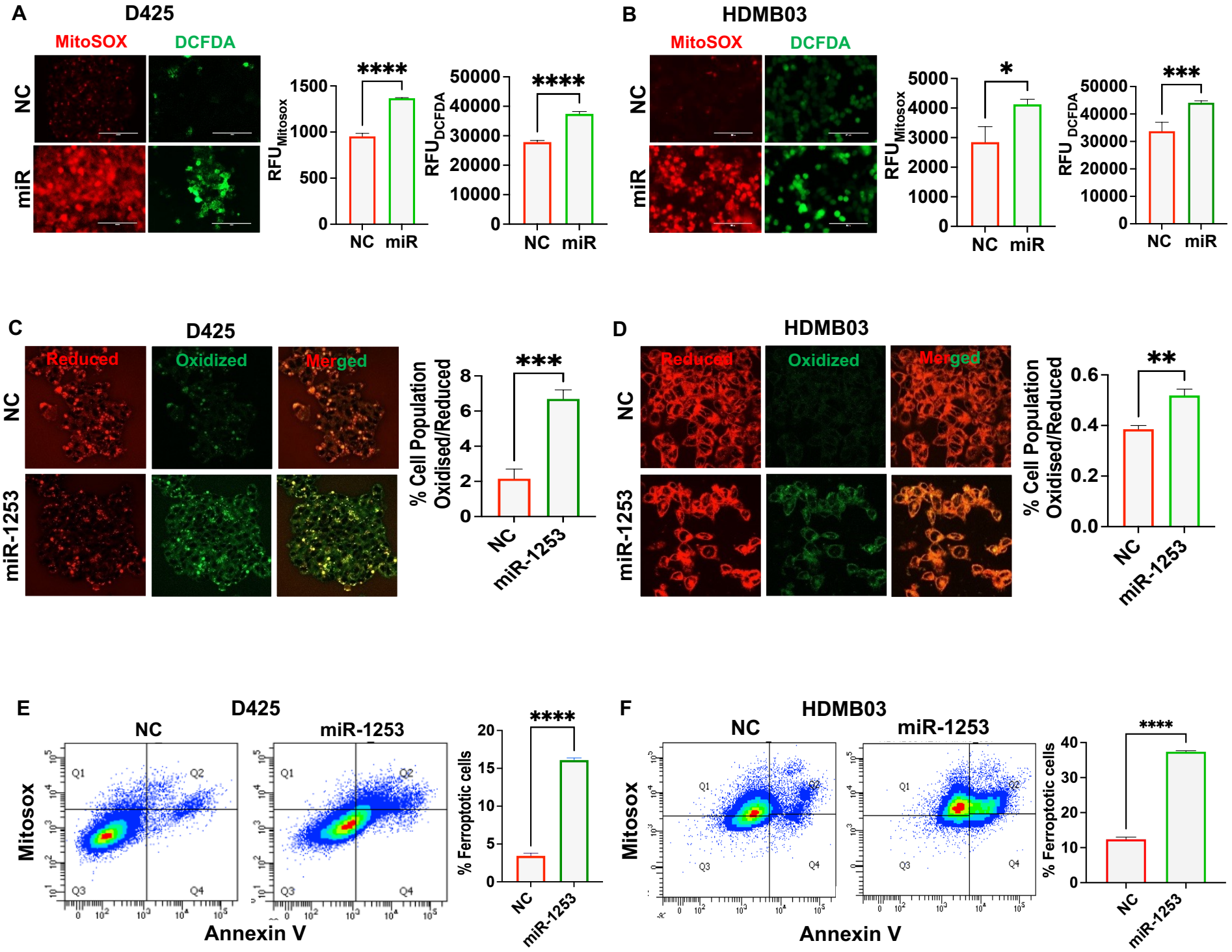
A
D425
MitoSOX
DCFDA
NC
miR
RFU Mitosox
RFU DCFDA
****
B
HDMB03
*
***
C
Reduced
Oxidized
Merged
miR-1253
% Cell Population Oxidised/Reduced
D
**
E
Mitosox
Annexin V
Q1
Q2
Q3
Q4
% Ferroptotic cells
F

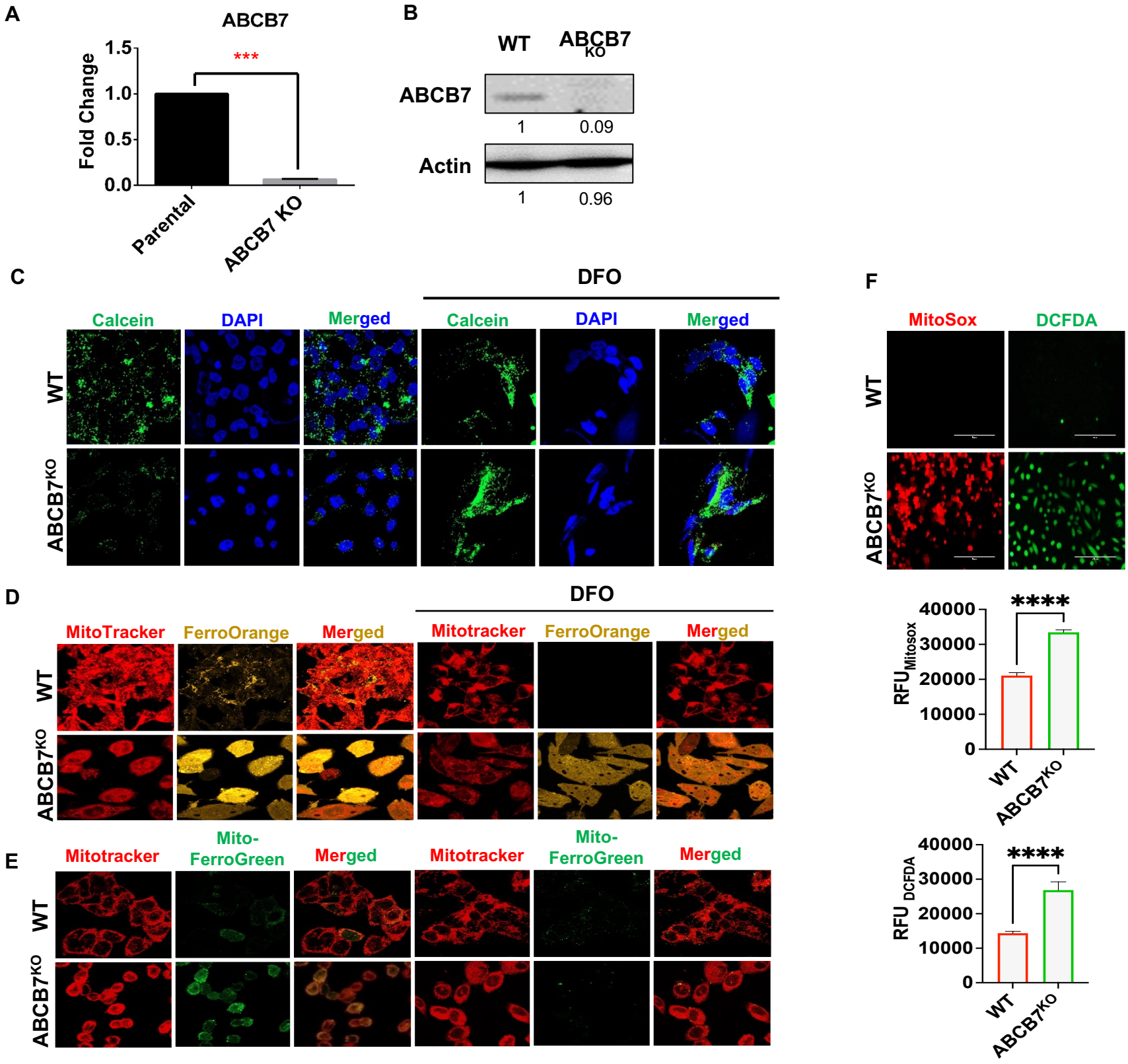
A
ABCB7
***
Fold Change
1.5
1.0
0.5
0.0
Parental
ABCB7 KO
B
WT
ABCB7 KO
ABCB7
1
0.09
Actin
1
0.96
C
DFO
Calcein
DAPI
Merged
Calcein
DAPI
Merged
WT
ABCB7KO
F
MitoSox
DCFDA
WT
ABCB7KO
D
DFO
MitoTracker
FerroOrange
Merged
Mitotracker
FerroOrange
Merged
WT
ABCB7KO
****
RFUMitosox
40000
30000
20000
10000
0
WT
ABCB7KO
E
Mitotracker
Mito-FerroGreen
Merged
Mitotracker
Mito-FerroGreen
Merged
WT
ABCB7KO
****
RFU DCFDA
40000
30000
20000
10000
0
WT
ABCB7KO

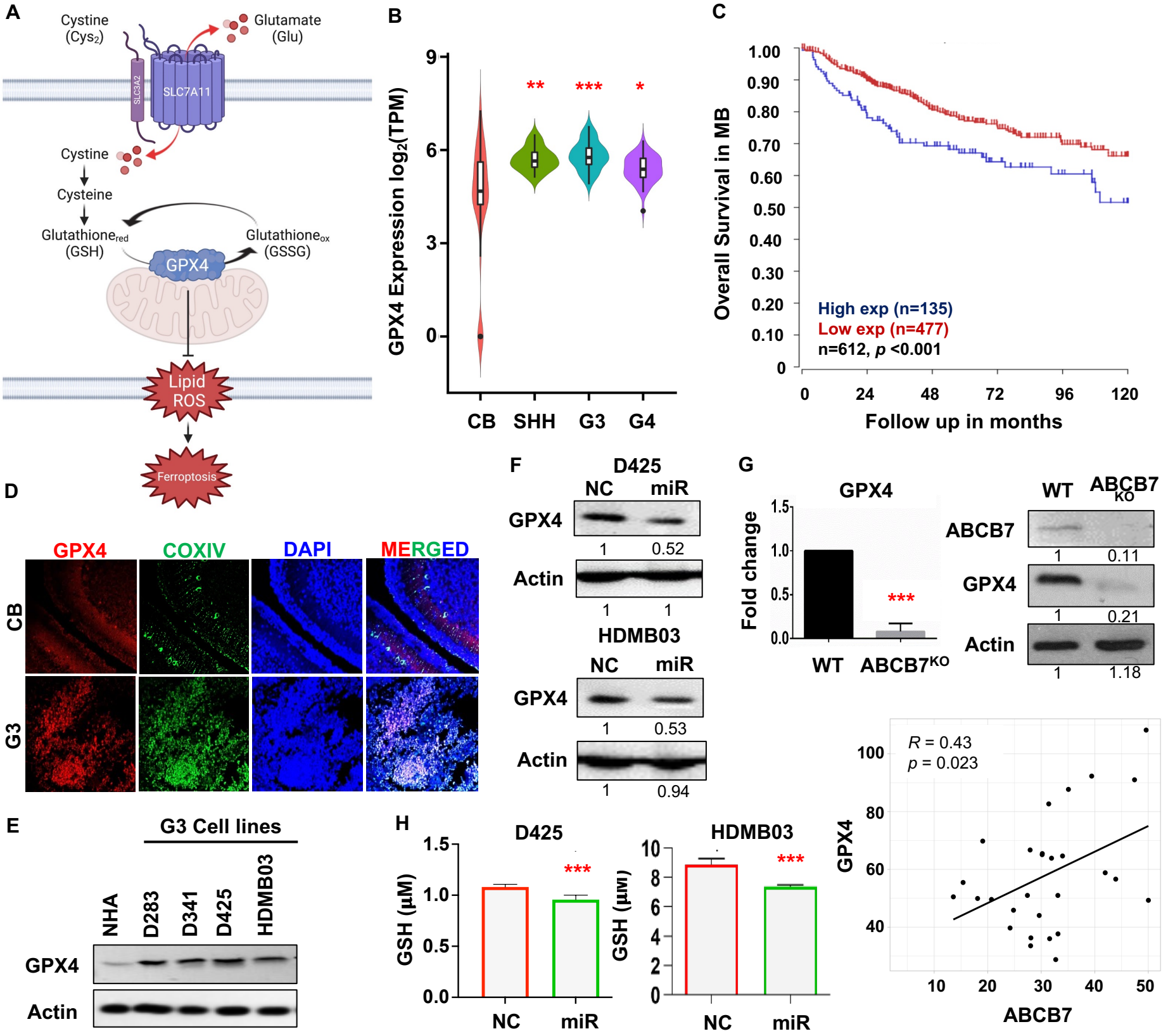
A
Cystine (Cys2)
Glutamate (Glu)
SLC3A2
SLC7A11
Cystine
Cysteine
Glutathionered (GSH)
Glutathioneox (GSSG)
GPX4
Lipid ROS
Ferroptosis
B
GPX4 Expression log2(TPM)
CB
SHH
G3
G4
C
Overall Survival in MB
High exp (n=135)
Low exp (n=477)
n=612, p <0.001
Follow up in months
D
GPX4
COXIV
DAPI
MERGED
CB
G3
E
G3 Cell lines
NHA
D283
D341
D425
HDMB03
GPX4
Actin
F
D425
NC
miR
GPX4
Actin
HDMB03
G
GPX4
Fold change
WT
ABCB7KO
ABCB7
H
D425
HDMB03
GSH (µM)
NC
miR
R = 0.43
p = 0.023
ABCB7

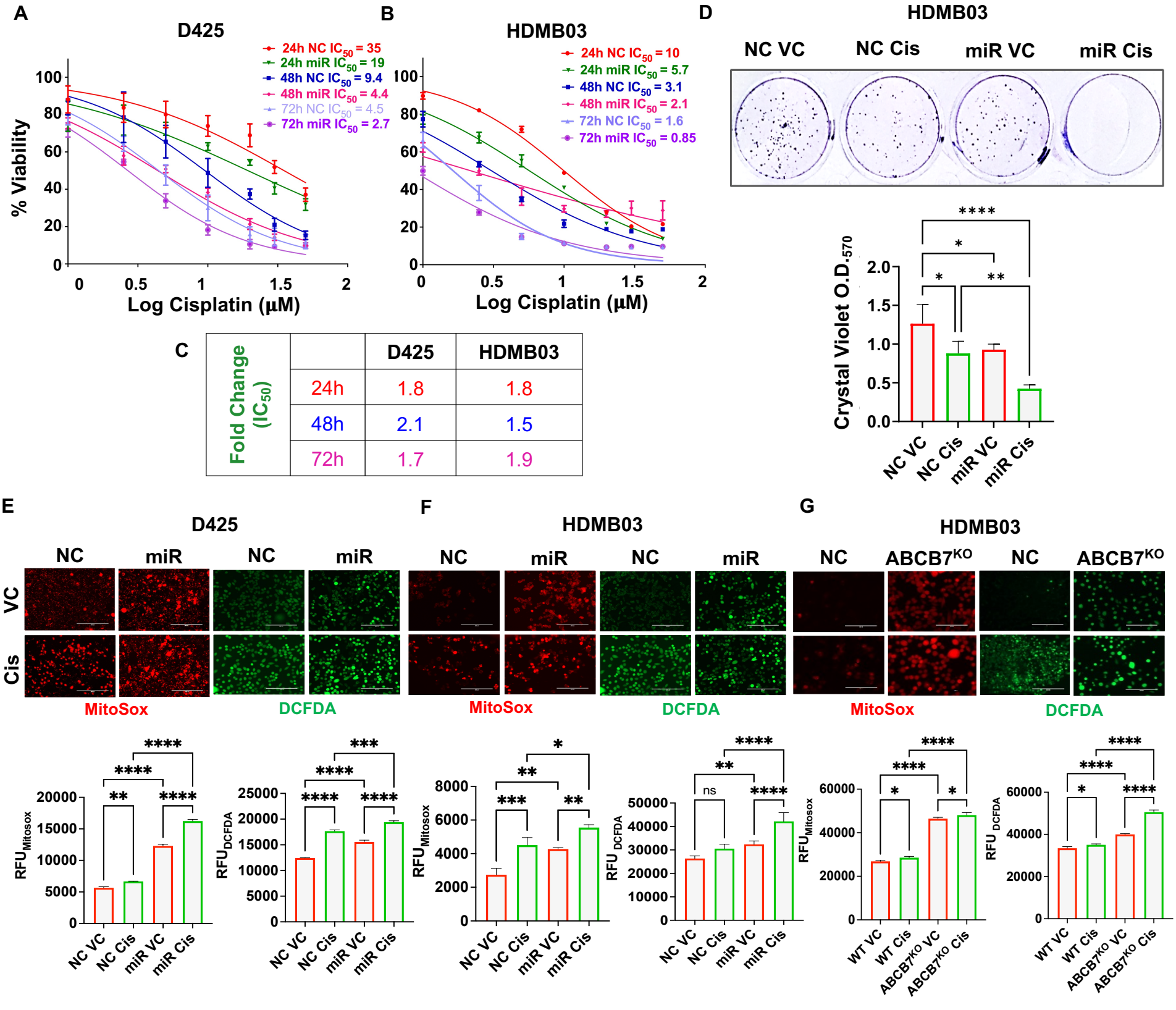
A
D425
24h NC IC50 = 35
24h miR IC50 = 19
48h NC IC50 = 9.4
48h miR IC50 = 4.4
72h NC IC50 = 4.5
72h miR IC50 = 2.7
% Viability
Log Cisplatin (µM)
B
HDMB03
24h NC IC50 = 10
24h miR IC50 = 5.7
48h NC IC50 = 3.1
48h miR IC50 = 2.1
72h NC IC50 = 1.6
72h miR IC50 = 0.85
Log Cisplatin (µM)
C
Fold Change (IC50)
D425
HDMB03
24h 1.8 1.8
48h 2.1 1.5
72h 1.7 1.9
D
HDMB03
NC VC
NC Cis
miR VC
miR Cis
Crystal Violet O.D.570
E
D425
NC
miR
VC
Cis
MitoSox
DCFDA
F
HDMB03
G
HDMB03
ABCB7KO
RFUMitosox
RFUDCFDA
WT VC
WT Cis
ABCB7KO VC
ABCB7KO Cis
ns

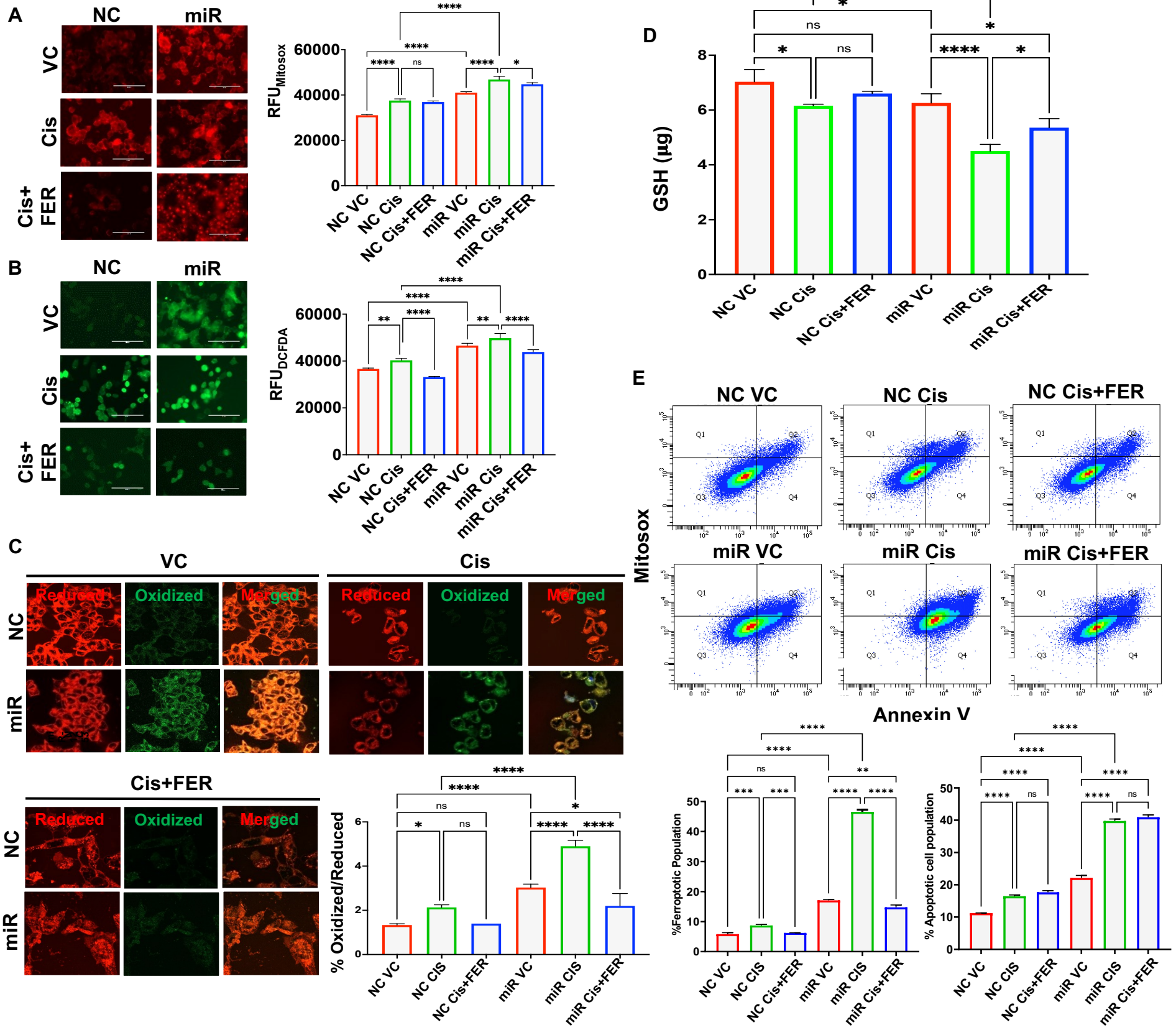
A
NC
miR
VC
Cis
Cis+ FER
RFU Mitosox
60000
40000
20000
0
NC VC
NC Cis
NC Cis+FER
miR VC
miR Cis
miR Cis+FER
B
RFU DCFDA
C
VC
Cis
Cis+FER
Reduced
Oxidized
Merged
% Oxidized/Reduced
D
GSH (µg)
E
Mitosox
Annexin V
%Ferroptotic Population
% Apoptotic cell population

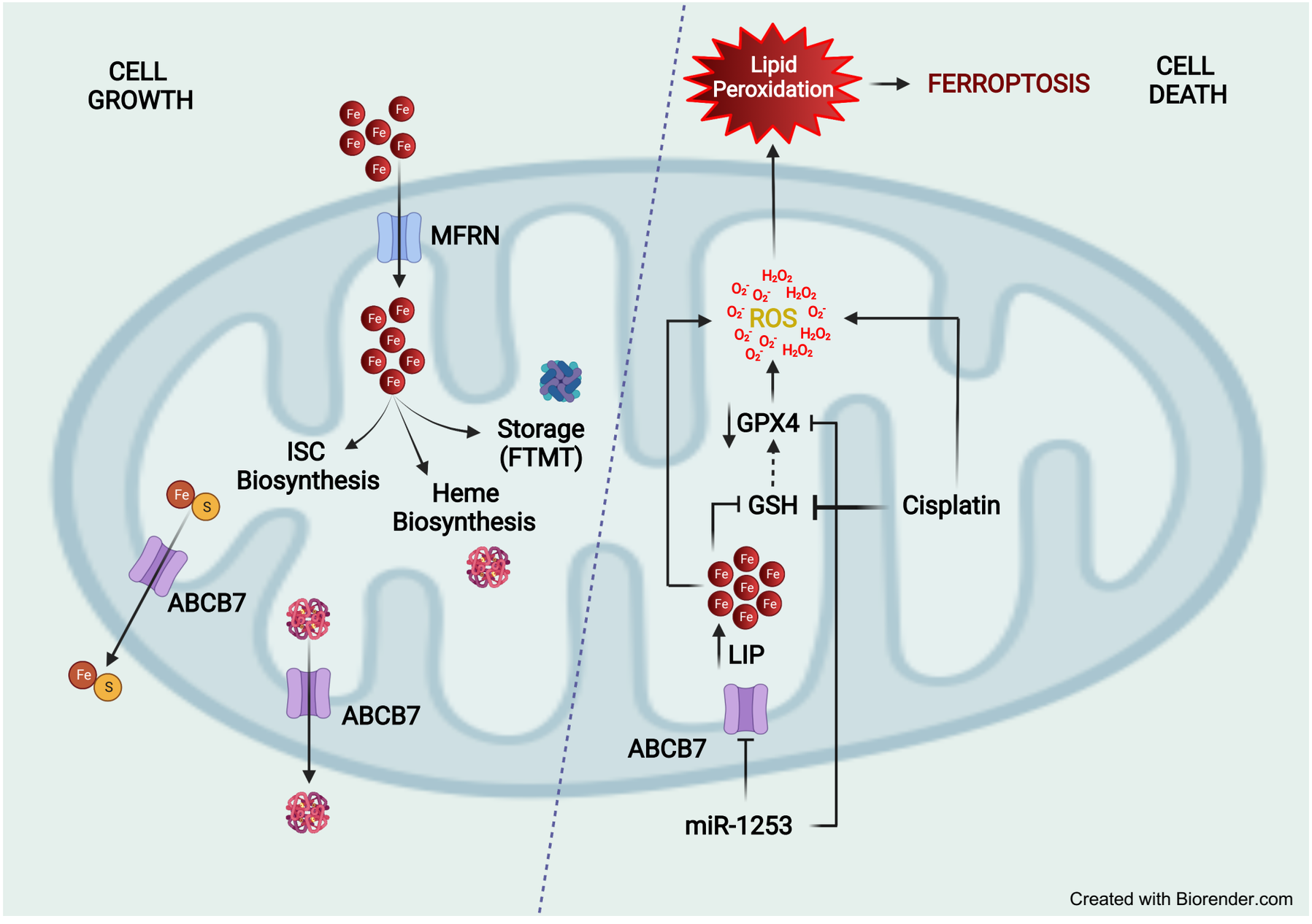

Schematic representation of miR-1253-induced ferroptosis. Under normal conditions, Fe^{2+} is imported into the mitochondria via the mitoferrin (MFRN) transporters for 3 primary purposes: i) Fe-S cluster (ISC) synthesis, ii) heme synthesis, or iii) storage as ferritin (FTMT). Fe-S clusters and heme are exported back to the cytoplasm via ABCB7 to fuel various cellular processes. In cancer, these transporters are deregulated resulting in abnormal iron transport facilitating tumor growth. Targeted inhibition of ABCB7 by miR-1253 results in generation of a labile free iron pools (LIP) resulting in elevated ROS; miR-1253 can also deplete glutathione (GSH) stores and inhibit glutathione peroxidase 4 (GPX4), a primary mitigator of ferroptosis. Cisplatin can work synergistically with miR-1253 by depleting GSH levels and inducing ROS to augment ferroptosis.